3-D seismic velocities calculated from lattice-preferred orientation and reflectivity of a lower crustal section: examples of the Val Sesia section (Ivrea zone, northern Italy)

Guilhem Barruol, David Mainprice

Geophys. J. Int. (1993) **115**, 1169–1188

3-D seismic velocities calculated from lattice-preferred orientation and reflectivity of a lower crustal section: examples of the Val Sesia section (Ivrea zone, northern Italy)

Guilhem Barruol and David Mainprice

Laboratoire de Tectonophysique, URA CNRS 1370, *Université Montpellier II*, 34095 *Montpellier cedex* 5, *France*

Accepted 1993 June 16. Received 1993 June 11; in original form 1992 June 3.

SUMMARY

To quantify the seismic properties of lower crustal rocks and to better constrain the origin of the lower crustal seismic reflectivity, we determined the complete 3-D seismic properties of a lower crustal section. Eight representative samples of the main lithologic and structural units outcropping in the Val Sesia (Ivrea zone) were studied in detail. The seismic velocities were calculated using the single crystal stiffness coefficients and the lattice preferred orientation (LPO) of each mineral in all samples. The 21 stiffness coefficients characterizing the elastic behaviour of each rock are determined. Mafic and ultramafic rocks such as pyroxenite and pyroxene-bearing gabbros display complex shear wave properties. These rocks are weakly birefringent (maximum 0.1 km s^{-1}) and it is difficult to find consistent relationships between the seismic properties and the rock structure. On the other hand, seismic properties of deformed felsic rocks are essentially controlled by mica. They display strong S-wave birefringence (0.3 km s^{-1}) and relatively high V_p anisotropy (7.6 per cent). Amphibole also strongly influences the rock birefringence patterns. For both kind of rocks, the foliation is highly birefringent and the fast polarized shear wave is systematically oriented parallel to the foliation. We show that the number of mineral phases in the rock strongly controls the anisotropy. The seismic anisotropy has a complex role in the P-wave reflectivity. Compared to the isotropic case, anisotropy enhances the reflection coefficient for about 60 per cent of the possible lithological interfaces. For 40 per cent of the interfaces, the reflection coefficient is much lower when one considers the medium as anisotropic.

Key words: anisotropy, crustal structure, Italy, seismic reflection, seismic velocities.

1 INTRODUCTION

The national seismic reflection programmes (BIRPS, COCORP, ECORS, DEKORP, CROP, NFP) have accumulated an enormous data base on the structure of the Earth's continental crust. More precise interpretations require more accurate knowledge of the behaviour of seismic waves in complex media and particularly in anisotropic materials. In this paper, we calculate anisotropic seismic properties of eight typical lower crustal rocks from a geological section that has a surface outcrop of 10×6 km. These calculations allow a complete evaluation of the effect of the composition and the structure of the rock on its complex elastic anisotropy. The origin of various seismic structures observed in seismic profiles (e.g. transparent sections, laminated, bright spot reflectors, etc.) can be evaluated using these data.

The 21 elastic constants characterizing the elastic behaviour of an anisotropic medium enable one to calculate seismic velocities in all directions using the Christoffel equation (e.g. Crosson & Lin 1971; Peselnick, Nicolas & Stevenson 1974). The P-wave velocity (V_p), the two shear wave velocities (V_{S_1} and V_{S_2}, $V_{S_1} > V_{S_2}$), the birefringence ($\Delta V_S = V_{S_1} - V_{S_2}$) and the orientations of the shear wave polarization planes can be calculated for each direction of propagation. The 21 stiffness coefficients of a monomineralic aggregate are determined from the lattice preferred orientation (LPO or textures), the single crystal stiffness coefficients and the aggregate density. For a polymineralic rock, one needs to measure the LPO of each rock-forming mineral phase. The whole rock elastic properties are then calculated from the rock density and from the six by six matrix of each monomineralic aggregate taken into account in its modal proportions. This approach provides the

opportunity to control the 3-D anisotropy by the three steps in the calculations: (1) seismic anisotropy of the single crystal, (2) seismic properties of each mineral phase, and finally (3) the influence of each mineral volume percentage on the total aggregate anisotropy. The details of such calculations have already been described by several authors (e.g. Siegesmund, Takeshita and Kern 1989; Mainprice, Casey and Schmid 1990a). A computer program has also been developed to do these calculations and to produce the spatial representation of the seismic velocities (Mainprice 1990). Petrofabric data may also be used to calculate other tensorial physical properties (e.g. conductivity, thermal expansion, etc.).

Particular attention has been paid to shear wave splitting in lower crustal rocks because it is an anisotropy-induced phenomenon: a shear wave crossing an anisotropic media splits into two perpendicularly polarized waves that propagate at different velocities (V_{S_1} and V_{S_2}, $V_{S_2} < V_{S_1}$). Using three-component seismic stations, one may measure the orientation of the polarization planes of the fast and slow split shear waves and the difference in arrival times. This delay time is an interdependent function of the anisotropy magnitude and the length of the anisotropic ray path. Such measurements may give first-order structural and geodynamic information (Silver & Chan 1988, 1991; Barruol & Mainprice 1993). Knowledge of the detailed seismic properties of anisotropic rocks are hence useful to constrain interpretations of shear wave splitting.

The determination of the 21 constants characterizing the elastic behaviour of anisotropic media is difficult by traditional laboratory methods which require numerous direct velocity measurements (Christensen & Crosson 1968; Seront, Mainprice & Christensen 1993). The use of petrofabric data for this type of study is possible because interactive programs are available which considerably reduce measurement time (e.g. Benn & Mainprice 1989). Using this second approach, this work presents the complete 3-D seismic properties of representative samples of a complex geological structure. When coupled with structural field observations (foliation and lineation), these data provide the means to study the seismic properties of the geological object in its actual orientation or in its assumed initial orientation in the lower crust (for example with the foliation horizontal). The 21 elastic constants may be used to simulate the seismic response using synthetic seismograms. It is also possible to extrapolate elastic properties to pressures and temperatures encountered in the lower crust using the appropriate derivatives.

For this study we used samples from the Ivrea zone, which has been the object of many seismic modelling studies (e.g. Fountain 1976; Fountain & Salisbury 1981; Fountain 1986; Hurich & Smithson 1987; Burke & Fountain 1990). For our detailed seismic modelling of a lower crust and a crust–mantle transition, we chose an east–west section through the Balmuccia massif and the basic intrusion between Val Mastallone and Val Sesia. This lower crustal section, although one of the best studied, cannot be generalized to the entire Ivrea zone and obviously not to every lower crustal situation. The northern part of the Ivrea zone (Val Strona and Valle d'Ossola), is lithologically different than the southern part (see Fig. 1) and is the object of a complementary study (Barruol & Kern 1993) combining

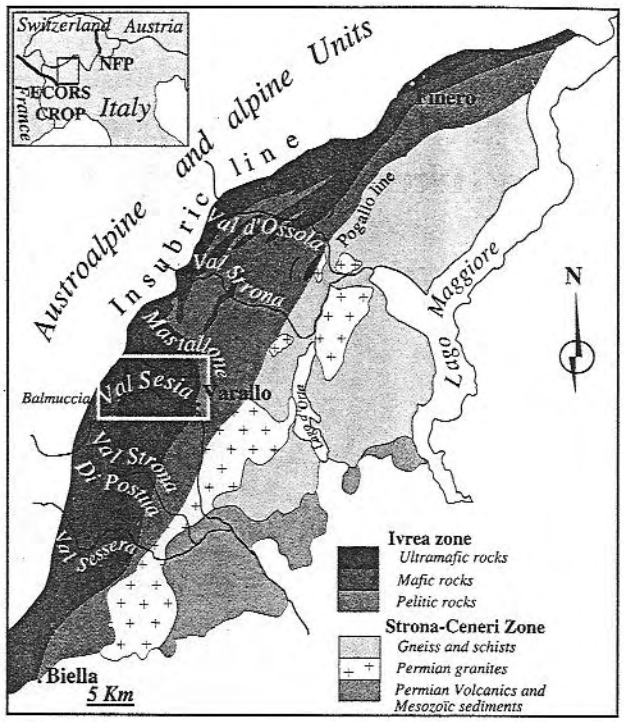

Figure 1. Schematic map of the Ivrea zone, modified after Zingg (1980), and location of the studied area. The NFP and ECORS profiles are located on the inset map.

calculations of seismic properties and direct velocity measurements.

The Ivrea Zone was selected for several reasons. (1) It is widely accepted that this area represents a lower crustal section. It experienced several tectonic episodes and is hence only a final state. (2) The outcrops are continuous over a large area. (3) The general structure, and the geophysical and petrological framework of this zone are relatively well defined by previous works. (4) The studied area is located between two seismic reflection profiles perpendicular to the strike of the belt. In the south, the ECORS-CROP profile has an E–W trend and in the north, the NFP profile is N–S (Fig. 1). The gravity and the seismic reflection studies provide some constraints on the geometry, density and seismic velocities of the lower crust in this region. (5) Finally, several authors selected the Ivrea zone to investigate the seismic properties of the lower crust by direct velocity measurements (e.g. Fountain 1976; Burke & Fountain 1990), but none using the calculation method from petrofabric data.

In the first part of this paper, we outline the geological characteristics of the Ivrea zone. In the second part we present the sample locations, the density measurements and the modal analyses that were used to characterize the various lithological units and to select representative samples in each. We examine, in the third part, the main features of the single crystal seismic properties and we briefly describe the methods of crystallographic measurements. We then present the calculated *P*-and *S*-wave seismic properties of the eight selected samples. In the final section of this paper, we discuss the factors controlling the *P*- and *S*-wave anisotropy and the influence of the seismic

anisotropy on the amplitude of the reflection coefficients of seismic body waves.

2 GEOLOGIC SETTING

The Ivrea zone, northern Italy, is the innermost Alpine zone. It is covered on its eastern side by the sediments of the Po plain and is abruptly limited on its western side by the Insubric Line (Fig. 1), a major lithospheric fault (Schmid, Zingg & Handy 1987). The mylonitic and cataclastic Insubric Line affects the western edge of the European plate and is an Alpine metamorphic and strain boundary. It is generally accepted that the Ivrea zone represents the northwestern boundary of the south Alpine plate (e.g. Zingg *et al.* 1990). Seismic and gravity anomalies suggest a mantle shallowing from 30 km under the Po plain to 3 km under the Ivrea zone (Berckemer 1968; Giese 1968). The Bouguer gravity anomaly displays an important positive anomaly associated with the Ivrea zone. Some recent gravimetric modelling combined with the ECORS-CROP vertical seismic reflection profile (Bayer *et al.* 1989; Rey 1989; Nicolas *et al.* 1990) confirm this mantle uplift.

Rocks from the lower crust and upper mantle (Ivrea zone) outcrop at the surface, as do rocks from middle to upper crust (Serie dei Laghi). The area gives the earth scientist the opportunity to observe a crustal section, particularly the lowest parts of the crust which are not normally exposed as a continuous sequence. The Ivrea zone and the adjacent Serie dei Laghi are separated by the Pogallo ductile fault in the north and the CMB line (Boriani, Burlini & Sacchi 1990) in the south (Fig. 1). The Pogallo vertical mylonite zone is interpreted as originally low-angle ductile normal faults which accommodated crustal thinning during the early Mesozoic (Hodges & Fountain 1984; Handy 1987). The extension could be due to the rifting between the European and south Alpine plate and the subsequent opening of the Alpine ocean. Other lower crustal shear zones in this region (particularly in the Val d'Ossola) are also interpreted as extensional structures (Brodie & Rutter 1987) and are thought to have initiated during the early Permian (Brodie, Rex & Rutter 1989). In the uppermost crustal levels, syntectonic Trias–Jurassic sedimentation in rift basins is the highest level manifestation of this crustal thinning (Kälin & Trümpy 1977).

Numerous events in the geological history of the Ivrea zone, for instance the origin of the granulitic and amphibolitic metamorphism, the formation of the basic intrusion, the dates and tectonic context of the peridotite massifs emplacements, have been and remain sometimes controversial (Köppel 1974; Hunziker & Zingg 1980; Zingg 1980; Pin 1986; Cumming, Köppel & Ferrario 1987; Zingg *et al.* 1990). The mafic intrusion seems to be contemporaneous with the granulitic metamorphism due to a mantle upwelling (Nicolas 1984; Zingg *et al.* 1990). Several authors interpret the high-temperature granulitic metamorphism and the underplating of magma in a simple extensional tectonic and metamorphic frame (Furlong & Fountain 1986; Fountain 1989). Recent and detailed structural studies give useful constraints on the complex history of this region (e.g. Brodie, Rutter & Evans 1992).

The westernmost part of the Ivrea zone (i.e. the deepest levels) is composed of several periodotite massifs (e.g. Baldissero, Balmuccia and Finero). The peridotites represent the subcrustal lithospheric mantle (Shervais 1979; Boudier, Jackson & Nicolas 1984). They were emplaced at the bottom of the crust at pressure and temperature conditions of about 800–1000 MPa and 800–900 °C (Shervais 1979) before the crust tilt. It is therefore possible to observe the original petrological Moho, defined as the interface between rocks with crustal composition (gabbros and pyroxenites) and mantle rocks *sensu stricto* (peridotites).

On a regional scale, the crustal section is lithologically different in the north and in the south (Fig. 1): in the southern part of the Ivrea zone (Val Mastallone, Val Sesia, Val Sessera), the peridotite massifs are overlain by a mafic to ultramafic banding such as pyroxenite, dunite and pyroxene- or garnet-bearing gabbros. These rocks equilibrated at high temperature are interpreted as underplated material (Shervais 1979; Fountain 1989). In the Val Sesia (Fig. 2), on the eastern side of the Balmuccia massif, this zone of mafic and ultramafic layered rocks has been defined as the Lower Layered Group (LLG) by Rivalenti *et al.* (1981) and is about 1 km thick. Gabbros of the LLG in the Val Sesia often display signs of plastic deformation. The LLG is overlain by a gabbroic to dioritic body, the Main Gabbros (MG) of Rivalenti *et al.* (1981) that intrude the overlying kinzigites (metasedimentary rocks metamorphosed in the amphibolite facies). This 8–10 km thick intrusion is interpreted as resulting from underplating of magma derived from subcontinental mantle partial melting (e.g. Pin & Sills 1986; Fountain 1989; Voshage *et al.* 1990; Brodie *et al.* 1992; Quick *et al.* 1992). In Val Sesia and Val Mastallone both regional foliation and layering are, on average, oriented N–S and vertical although displaying a regional curvature (Quick *et al.* 1992). In the northern Ivrea zone (Val Strona, Val d'Ossola, Val Cannobina) the lowermost parts of the crust are composed of granulitic and amphibolitic paragneisses (stronalites and kinzigites) interlayered with amphibolites, garnet-bearing gabbros, metagabbros and marbles.

Measurements of metamorphic temperature and pressure conditions in metabasic rocks and metapelitic gneisses in the Val Sesia were estimated in the range 700–800 °C at 800 MPa by Schmid & Wood (1976) and about 600–900 °C at 800–900 MPa by Hunziker & Zingg (1980). Sills (1984) determined the metamorphic temperature to be about 750 °C at 600 MPa in the Val Strona, but described a continuous pressure gradient along an E–W transect through the Ivrea zone. For example, in the Val Sesia the pressures were estimated to have reached 600 MPa in Varallo and 850 MPa in the Balmuccia peridotite massif. The metamorphic grade systematically increases westward, normal to general strike of the structure, from the amphibolite facies to the granulite facies (Hunziker & Zingg 1980; Zingg 1980).

3 SAMPLE SELECTION

To model the seismic properties of this particular lower crustal section as realistically as possible, the different representative units were extensively sampled (about 150 samples). Density and modal composition measurements allowed us to have more quantitative data characterizing the geological body. The systematic analysis of thin sections

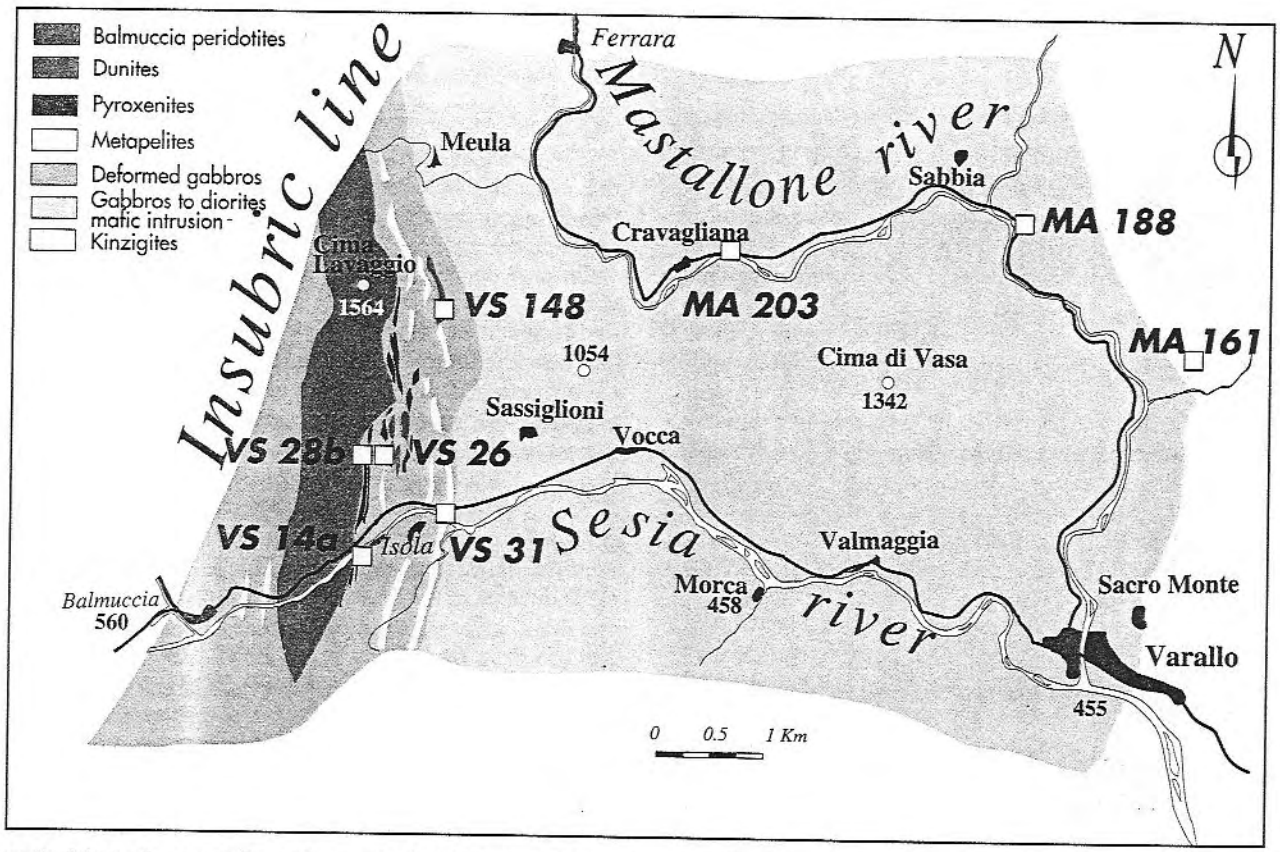

Figure 2. Schematic map of the study area in the Val Sesia and Mastallone, modified after Rivalenti *et al.* (1981). The main petrographic units are distinguished. The eight samples on which the complete petrofabric measurements were performed are located by the open squares. The regional foliation in this area is oriented N–S and vertical.

combined with the rock densities and compositions enabled us to select eight typical lower crustal rocks on which crystallographic measurements were performed (Table 1).

3.1 Density measurements

Rock densities were systematically determined by weighing the samples dry and then in water-saturated conditions. The location map (Fig. 3a) shows that the sampling has been relatively uniform and homogeneous through the different units. The density diagram (Fig. 3b) may hence be considered as representative of this crustal section. The density generally increases to the west, toward the petrological Moho as defined by the gabbro–peridotite interface. But, at any given distance, the rock densities scatter. This scatter reflects the fine-scale layering visible in the field, such as the pyroxenite ($d = 3.2\,\mathrm{g\,cm^{-3}}$) and anorthosite ($d = 2.8\,\mathrm{g\,cm^{-3}}$) banding, for instance. We distinguished three principal trends: (i) between 10 and 8 km (arbitrary origin at the Insubric line) density steadily increases from 2.6 to 2.9 $\mathrm{g\,cm^{-3}}$. This represents the base of the metamorphic rocks (kinzigites, quartz-rich paragneisses, marbles) and the top of the basic intrusion (diorites). (ii) Between 8 and 4 km, the density is more or less constant (in the range 2.9–3.0 $\mathrm{g\,cm^{-3}}$) and corresponds to the homogeneous gabbroic basic intrusion. (iii) Between 4 and 2 km the density steeply increases from 2.9 to 3.4 $\mathrm{g\,cm^{-3}}$. This corresponds to the LLG in which layering becomes ultramafic (pyroxenites, dunites). The gap in the data (from 2 to 1 km) corresponds to the Balmuccia peridotite massif, which was not intensively sampled. On the western side of the Balmuccia massif, the density decrease is roughly symmetrical with the eastern side. The values are in fact slightly lower due to the presence of the Insubric line and its associated greenschist facies metamorphism minerals.

3.2 Modal analysis

Rock modal compositions were determined by image analysis of thin sections using a microcomputer (Allard & Sotin 1988). All the units were studied. Only results for plagioclase and pyroxene are presented (Fig. 3c) because they represent the major proportion of the rock volume. These two minerals are classically described as important lower crustal phases that may control the physical behaviour of the lower crust and hence its rheology and seismic properties. From W to E, the plagioclase content strongly increases in the LLG (from 0 to 60 per cent) and is approximately constant (50–60 per cent) within the basic intrusion. The pyroxene content decreases steadily from 90 per cent in the LLG to about 0 per cent at the top of the basic intrusion. The main gabbro and diorite body has to a first approximation a relatively homogeneous composition (60 per cent plagioclase and 40 per cent pyroxene). Sample density (Fig. 3b) correlated fairly well with pyroxene content.

Table 1. Density, mineral composition and summary of microstructures of the eight selected samples.

Lithology	Sample number	Density g/cm3	Modal composition (%)	Microstructures
				Abbreviations: Text.=texture, GS=grain size, SR=shape ratio, opx=orthopyroxene, cpx=clinopyroxene, plagio=plagioclase, ol=olivine, spi=spinel, amph= amphibole, gar=garnet, op=opaques
Pyroxenite	87VS28b	3.37	45 cpx., 45 opx., 10 op.	Mesocumulat text., opx and cpx subeuhedral, no elongated grains, some folded lattices. No recrystallization.
Dunite	87VS148	3.38	95 oliv., 5 spi.	Polygonal text. ol. grain size 2-3 mm, 120° triple junctions, numerous undulose extinction. Elongated spi. included in ol.
Sheared pyroxenite	87VS14a	3.21	65 cpx., 25 plagio., 10 gar.	Porphyroclastic text. Ribbon plagio., SR up to 4, numerous undulose extinctions, tapered twins, typical GS 3 by 1 mm. Elongated pyrox., but SR<3, some kinked and broken lattices. Slight recrystallization at grain boundaries.
Sheared gabbro	87VS26	3.17	30 plagio., 20 opx., 20 cpx., 25 gar., 5 op.	Porphyroclastic text. Very elongated grains, GS 4 mm long. Ribbon plagio., SR up to 8, numerous folded lattices. Ribbon pyrox. SR up to 4. Few recrystallization
Stronalite	87VS31	2.88	45 plagio., 25 opx., 15 quartz, 12 gar., 3 op.	Porphyroclastic text. plagio. and pyrox. are elongated but with SR<2, GS up to 2mm. Ribbon quartz, several cm long, but recrystallised, new grains 0.2 to 0.4 mm, serrated subgrain boundaries.
Magmatic gabbro	87MA203	2.77	75 plagio., 22 opx., 3 others (biot.,amph.)	Magmatic and equigranular text. Euhedral plagio. grains, GS up to 5mm, typically magmatic twins, no undulose extinction. Euhedral opx grains underlying a weak lineation. No recrystallization.
Diorite	87MA188	2.93	65 plagio., 7 opx., 8 cpx., 10 amph., 10 biot.	Heterogranular text. Weak foliation and lineation. Subeuhedral plagio. grains, GS 1 to 5 mm, straight sided albite twins, no undulose extinction. opx euhedral. amph. grains interstitial. Foliation underlined by biotite crystals.
Kinzigite	87MA161	2.70	55 plagio., 25 quartz, 20 biot.	Grano-lepidoblastic text. plagio. grains subeuhedral to xenomorph, sometimes amigdaloid, GS between .5 and 3.0 mm. quartz globular shaped. Foliation underlined by biotite crystals.

4 CRYSTALLOGRAPHIC MEASUREMENTS AND SINGLE CRYSTAL SEISMIC PROPERTIES

Before discussing results of *P*- and *S*-wave seismic property calculations for each sample (next section), it is first useful to define the seismic velocities for a single crystal for each mineral phase encountered in this lower crustal section. Here we first explain how seismic properties may be calculated and then briefly outline, for each mineral, the method of crystallographic measurement that allows us to measure the complete textures of the eight selected samples (see Fig. 4), i.e. the method by which crystallographic orientations are deduced from optical measurements. The main features of the single crystal seismic properties are also summarized.

4.1 Seismic property calculations

Determination of *single crystal* seismic properties (V_p, V_{S_1}, V_{S_2}, seismic birefringence, orientation of the shear wave polarization planes) is based on the knowledge of the six by six stiffness matrix, the density, and by use of the Christoffel equation (e.g. Crosson & Lin 1971). In a *monomineralic aggregate,* the LPO (or texture) provides a means for the determination of the 21 elastic coefficients (the six by six symmetric matrix) characterizing the aggregate elastic behaviour. For each measured grain, the elastic matrix is rotated from the crystallographic to the rock reference frame (Peselnick *et al.* 1974). The aggregate elastic matrix is the average of the matrices of all grains. To calculate elastic properties of a *polymineralic rock,* the corresponding matrix of each monomineralic aggregate is taken into account in its modal proportion. The details of such calculations have already been described by numerous authors (e.g. Peselnick *et.al.* 1974; Siegesmund *et al* 1989).

P-wave phase velocity distribution in the selected rock-forming minerals are presented in Fig. 5 (left). The *P*-wave anisotropy coefficient is defined as $100 * (V_{max} - V_{min})/V_{P_{mean}}$ with $V_{P_{mean}} = (V_{max} + V_{min})/2$. This coefficient is only defined by the maximum and minimum velocity values and does not carry any information about their orientations. The mineral phases that occur in the lower crust all have strong *P*-wave anisotropies ranging from 12 per cent (enstatite) to 57 per cent (biotite).

Single crystal 3-D *S*-wave seismic velocities are also presented in Fig. 5. For each propagation direction the birefringence $\Delta V_S = V_{S_1} - V_{S_2}$ is calculated. The birefringence anisotropy, defined as $100 * (V_{S_1} - V_{S_2})/V_{S_{mean}}$ with $V_{S_{mean}} = (V_{S_1} + V_{S_2})/2$ is also presented in Fig. 5 (middle). *S*-wave anisotropy is therefore a directional parameter. V_S anisotropies range from 11 per cent (enstatite) to 72 per cent (biotite). Fig. 5 (right), displays the orientations of the fast shear wave polarization plane orientation.

All crystallographic measurements of each mineral phase of the selected samples were performed using an optical

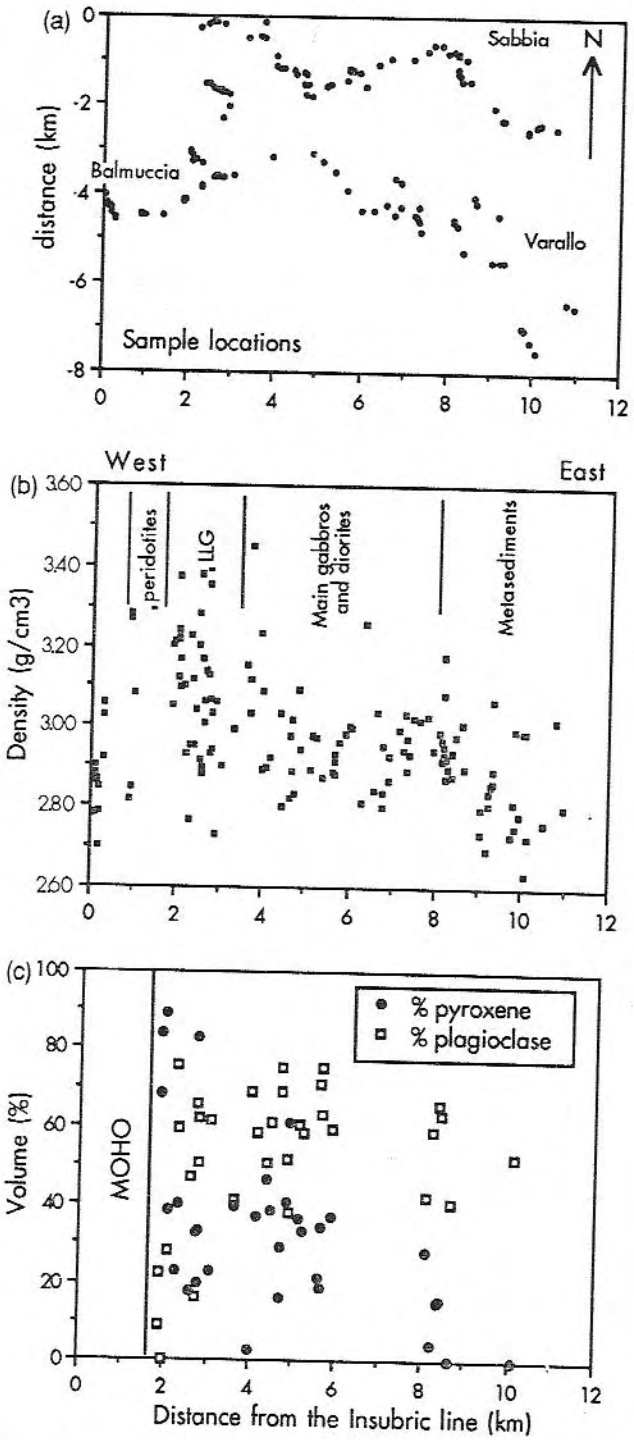

Figure 3. Location map of (a) all sampled rocks and (b) their measured densities. This second diagram is a projection of densities on an E–W plane (arbitrary origin at the Insubric line). Most of the samples were taken along the river beds. (c) Plagioclase (open squares) and pyroxene (solid circles) content of 33 typical samples: the vertical axis represents the volume percentage of those minerals and the horizontal axis the distance from the Insubric line (as in b). The plagioclase content is almost constant between 3 and 9 km (i.e. within the mafic intrusion) whereas it varies greatly in the lowermost crustal levels due to the intense mafic–ultramafic banding. The pyroxene content is very high in the lowermost part of the crust and decreases steadily in the upper levels. Note the good correlation between the pyroxene content and the density.

microscope equipped with a five-axis universal stage. Results are displayed in Fig. 4. More complete rock and LPO descriptions and detailed analyses may be found in Barruol (1993). For consistency, all LPOs are shown in pole figures in the XZ section orientation (Fig. 4), even if measured in a thin section with a different orientation. The structural planes in which measurements were performed are noted together with the number of measured grains in Table 2.

4.2 Single crystals properties

4.2.1 Olivine

Olivine has an orthorhombic crystallographic symmetry and is optically biaxial. The optical axes directly correspond to the main crystallographic axes: Ng = [100] = **a**, Np = [010] = **b** and Nm = [001] = **c**.

Olivine stiffness constants were taken from Kumazawa & Anderson (1969). High *P*-wave velocity (9.9 km s^{-1}) corresponds to the **a** crystallographic direction and slow V_p (7.7 km s^{-1}) to the **b** direction. The V_p anisotropy is relatively high (24 per cent). The maximum *S*-wave birefringence anisotropy (18 per cent) is located between the **a** and **c** axes. Zero birefringence is observed parallel to the **a** axis. All the fast shear wave polarization planes are co-zonal with the **a** axis.

4.2.2 Orthopyroxene

Orthopyroxene in these rocks is mostly hypersthene. Each optical indicatrix corresponds to a crystallographic axis due to its orthorhombic crystallographic symmetry: Np = [010] = **b**, Nm = [100] = **a** and Ng = [001] = **c**.

Orthopyroxene met in the studied rocks has a composition close the enstatite pole (composition of $Mg_{0.8}Fe_{0.2}SiO_3$ by Rivalenti *et al.* 1981). We therefore used the elastic constants determined for enstatite by Weidner & Vaughan (1982). The *P*-wave anisotropy is weak (12 per cent). Slow V_p (7.3 km s^{-1}) corresponds to the **b** crystallographic direction and the high V_p (8.2 km s^{-1}) to the **a** direction. The minimum *S*-wave birefringence defines a girdle containing the **a** and **c** crystallographic axes. Four zones of maximum birefringence (11 per cent) are located between the **b** and **a** axes. The associated polarization planes are oblique to the main crystallographic planes.

4.2.3 Quartz

Only the **c** crystallographic axis was measured. The two quartz-bearing rocks (the stronalite and the kinzigite) do not contain large amounts of quartz (15 and 25 per cent respectively). The quartz **c** axes are furthermore poorly organized. As a result, the quartz has been considered as randomly oriented and the isotropic quartz seismic properties (Kammer, Pardue & Frissel 1948) were used.

We nevertheless present the quartz single crystal anisotropic seismic properties (Fig. 5) calculated from stiffness coefficients obtained by Zubov & Firsova (1962). They are displayed in the α and β stability field. In the α-field (below 573 °C, here at 510 °C and at atmospheric

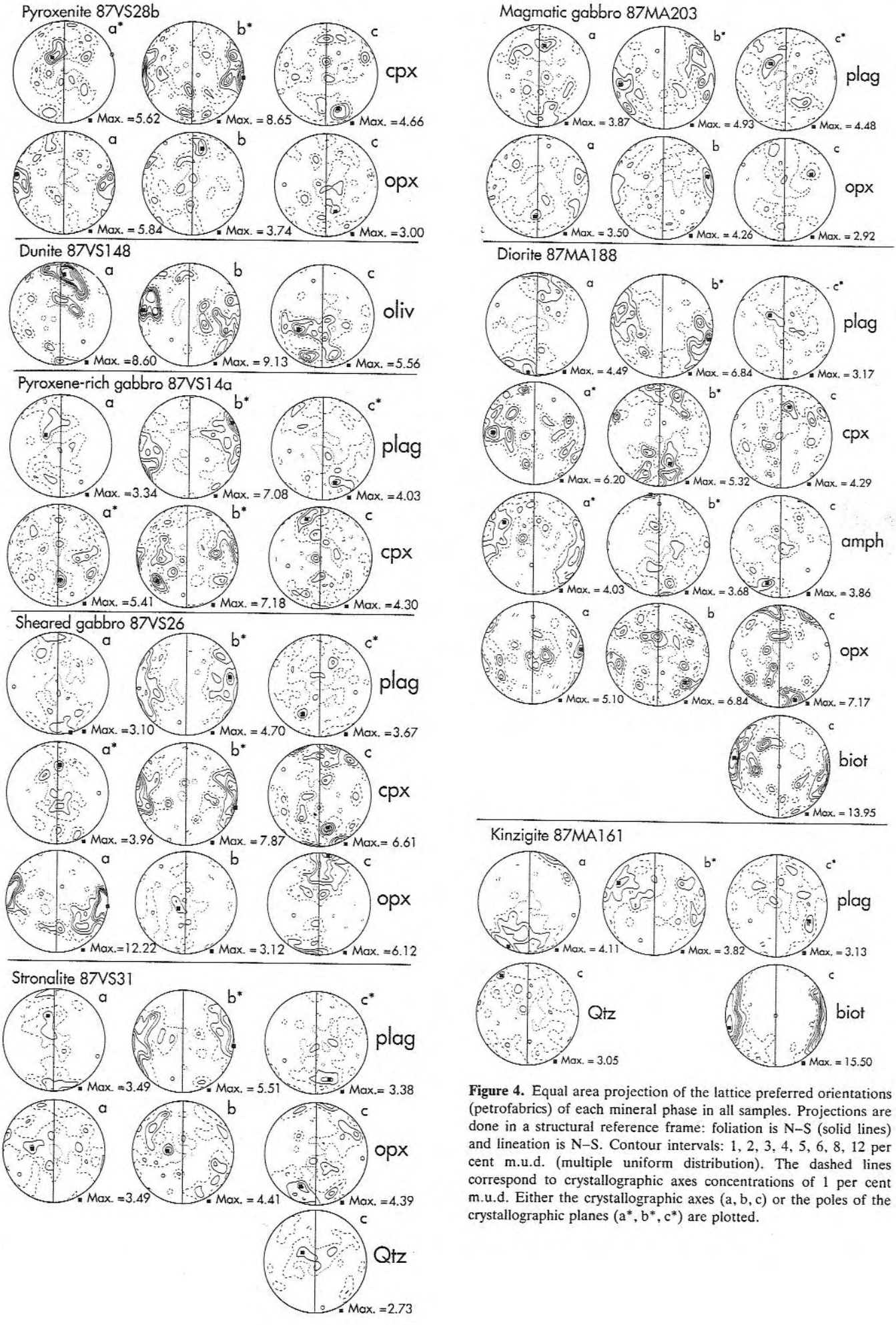

Figure 4. Equal area projection of the lattice preferred orientations (petrofabrics) of each mineral phase in all samples. Projections are done in a structural reference frame: foliation is N–S (solid lines) and lineation is N–S. Contour intervals: 1, 2, 3, 4, 5, 6, 8, 12 per cent m.u.d. (multiple uniform distribution). The dashed lines correspond to crystallographic axes concentrations of 1 per cent m.u.d. Either the crystallographic axes (a, b, c) or the poles of the crystallographic planes (a*, b*, c*) are plotted.

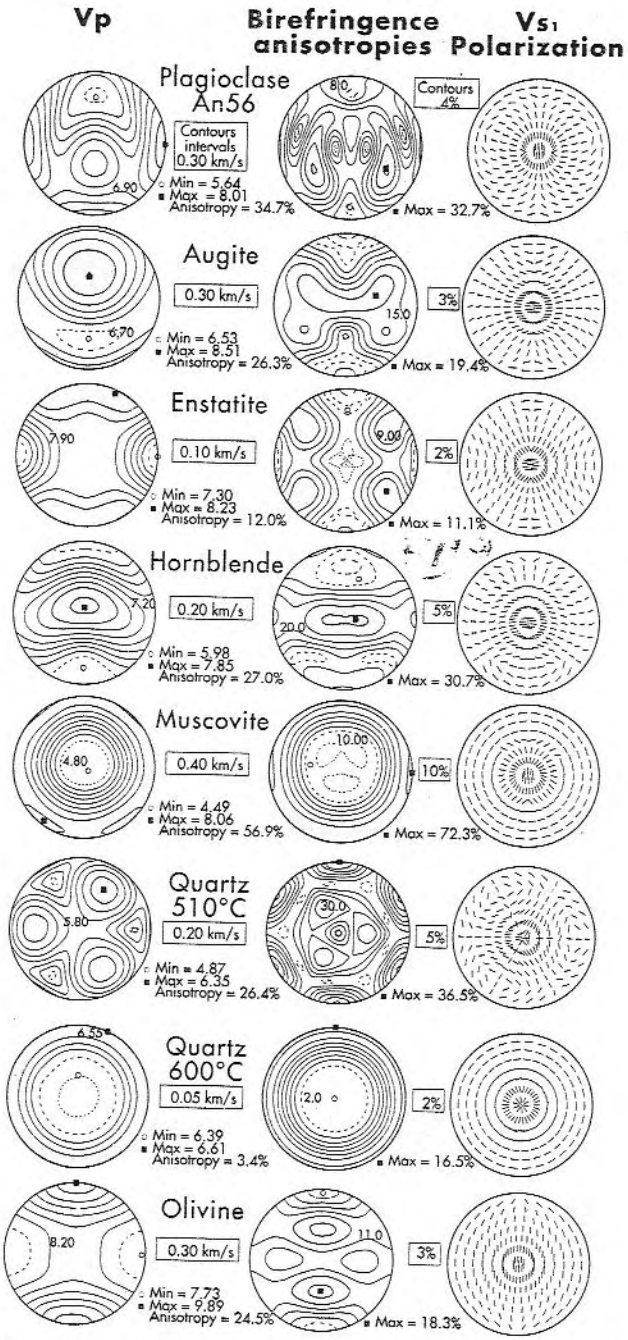

Figure 5. *P*- and *S*-wave properties of minerals that occur in the Val Sesia selected samples, the *P*-wave phase velocities (left), the *S*-wave birefringence anisotropies (as defined in the text) (middle), and the *S*-wave polarization plane orientations (right) are shown in equal area projection. For each propagation direction the small arc segment is a part of the great circle corresponding to the orientation of the polarization plane of the fast shear wave. The maximum velocity (in km s^{-1}) or anisotropy (in per cent) is marked by a solid square and the minimum by an open circle. Notice that the contour intervals are not the same for every diagram. Single crystal orientation is the following: North represents the crystallographic direction **a** or [100] for orthorhombic minerals. For monoclinic and triclinic minerals it corresponds to the **a*** direction (the pole of the (100) plane). The vertical direction corresponds to the **c** or [001] axis (orthorhombic minerals) or the normal to the (001) planes, or **c*** directions, for triclinic and monoclinic minerals. Shaded areas correspond to directions of high V_p or high birefringence anisotropies.

confining pressure) quartz displays a trigonal symmetry around the **c** axis and a complex topology of maxima and minima. The highest shear wave birefringence anisotropies (36 per cent) are parallel to the **a** and **m** axes. The **c** crystallographic direction corresponds to a three-fold axis. Quartz in the β field (above 573 °C, here at 600 °C and at atmospheric confining pressure) is transversely isotropic. The **c** crystallographic axis is the symmetry axis and corresponds to the minimum *P*-wave velocity (6.4 km s^{-1}) and to the minimum shear wave birefringence anisotropy. The α–β quartz phase transition considerably lowers the *P*-wave anisotropy (from 26 to 3 per cent) and the maximum shear wave birefringence decreases from 36 to 16 per cent (e.g. Mainprice, Humbert & Wagner 1990b).

4.2.4 *Biotite*

Biotite has a monoclinic crystallographic symmetry but its seismic properties are almost symmetric around the **c** axis (i.e. nearly transverse isotropic), due to the small deviation of the monoclinic crystal structure from hexagonal symmetry. Knowledge of the **c** axis orientation is sufficient to determine the complete seismic properties of biotite in the hexagonal symmetry approximation. Only the biotite cleavage planes (001) were measured, because complete LPOs of biotite are optically difficult to obtain. The **a** and **b** axes were assumed to be randomly distributed in the basal plane.

Muscovite single crystal stiffness constants that we used were determined by Vaughan & Guggenheim (1986). The crystallographic symmetry is monoclinic but displays an important axial symmetry around the **c** axis. Seismic properties of phyllosilicate aggregates mainly depend on the **c** axes orientations. Seismic waves propagate more quickly within phyllosilicate sheets than normal to them. Minimum *P*-wave (4.5 km s^{-1}) is parallel to the **c** axis whereas *P* waves propagate at the maximum velocity (8.1 km s^{-1}) in directions normal to the **c** axis. *P*- and *S*-wave anisotropies are extremely high (57 and 72 per cent respectively). The birefringence anisotropy is maximum for waves propagating and polarized parallel to the phyllosilicate sheet. Furthermore, for highly birefringent directions, the fast shear waves systematically polarize parallel to the sheet.

4.2.5 *Monoclinic crystals: clinopyroxene and amphibole*

For monoclinic minerals, determination of optical indicatrix does not directly allow determination of the complete crystallographic orientation. To determine the crystallographic orientation, the optical indicatrix and a crystallographic plane orientation, such as a (110) or (100) cleavage plane, are needed. The only Nm optical indicatrix corresponds to a crystallographic axis (the [010] or **b** direction). In this study, clinopyroxene measurements were systematically performed in the three structural planes (XZ, YZ, XY, X = lineation, Z = pole of the foliation) in order to try to minimize the problem of grain selection. In the XZ and YZ structural sections, numerous grains were unmeasurable because there was no visible measurable cleavage. On the other hand, in the XY plane (i.e. the foliation plane), more than 90 per cent of grains were

Table 2. Information on the crystallographic measurements performed on the eight selected samples: structural plane in which measurements were performed (X = lineation, Z = pole of the foliation) and number of measured grains.

	87VS28b Pyroxenite	87VS148 Dunite	87VS14a Sheared pyroxenite	87VS26 Sheared gabbro	87VS31 Stronalite	87MA203 Magmatic gabbro	87MA188 Diorite	87MA161 Kinzigite
Plagioclase	—	—	XZ+YZ 193 grains	XZ+YZ 210 grains	XZ+YZ 193 grains	XZ+YZ 202 grains	XZ+YZ 205	XZ+YZ 212 grains
Clinopyr.	XY 111 grains	—	XY 100 grains	XY 100 grains	—	—	YZ 78 grains	—
Orthopyr.	XY 108 grains	—	—	XZ 100 grains	XZ+YZ 160 grains	XZ+YZ 194 grains	XZ 188 grains	—
Amphibole	—	—	—	—	—	—	XZ+YZ 140 grains	—
Biotite	—	—	—	—	—	—	XZ 91 grains	XZ 150 grains
Olivine	—	XZ 100 grains	—	—	—	—	—	—
Quartz	—	—	—	—	XZ 275 grains	—	—	YZ 250 grains

measurable. Clinopyroxenes data presented in this work were therefore measured in the XY section.

Clinopyroxene elastic constants were determined by Aleksandrov *et al.* (1964) for augite and by Levien, Weidner & Prewitt (1979) for diopside in the diorite 188. Velocity distributions for these two minerals and the V_p anisotropy coefficients are very similar (26 and 29 per cent respectively) although diopside displays higher overall velocities than augite. Only the augite seismic properties are displayed in Fig. 5. The maximum augite *P*-wave velocity (8.5 km s^{-1}) is located between the **a*** and **c** axes. The maximum *S*-wave birefringence anisotopy is relatively high (19 per cent) but does not correspond to a low index crystallographic direction. The birefringence pattern is complex and exhibits two maxima between the **a*** and **c** axes. The fast shear wave also displays complex polarization patterns; no simple trends that could be directly related to the crystallographic axes.

Amphibole elastic constants used in our calculations are taken from Aleksandrov and Ryzhova (1961). The seismic properties display a high *P*-wave anisotropy (27 per cent). V_p minimum (6.0 km s^{-1}) is close to the **a*** direction and the maximum V_p (7.9 km s^{-1}) is oriented close to the **c** axis. *S*-wave birefringence anisotropies are low (<5 per cent) parallel to the **a*** axis and high along the **c** axis (31 per cent). A girdle of high birefringence anisotropies (>20 per cent) corresponds to the (100) crystallographic plane. Furthermore, the fast shear wave polarization planes for these directions of strong birefringence are systematically oriented parallel to the (100) plane. This has important consequences on seismic properties of amphibole-rich rocks.

4.2.6 *Plagioclase*

Plagioclase is a triclinic mineral, so the optical axes do not correspond to low index crystallographic directions. The crystallographic orientations of plagioclase may be determined combining the measurements of the optical indicatrix with two crystallographic planes: the (001) and (010) cleavages or the albite and pericline twin planes if the composition is unknown and the measured planes are unrecognizable. The geometric construction using the Burri diagram (Burri, Parker & Wenk 1967) allows the determination of the crystallographic orientation. This method is often selective because grains have not systematically the two crystallographic planes in observable orientations. Measurements were simplified in this work using only one crystallographic plane. This can be done when; (i) the plagioclase composition is known and (ii) the crystallographic identity of the measured plane can be determined. Using twins, the plagioclase composition may be easily determined by the extinction angle around the albite twin. A distinction between albite and pericline twins may be made using the symmetry of extinction. Plagioclase measurements were systematically carried out in two perpendicular structural sections: XZ and YZ, with about 100 grains measured in each section (see Table 2). Less than 10 per cent (and often less than 5 per cent) of the grains did not exhibit any measurable crystallographic plane and were not taken into account. LPOs obtained in each section display very similar patterns thereby indicating that the measurements were representative. Results from the two thin sections are grouped together and shown in the XZ frame in an equal area projection (Fig. 4). The fastidious manipulations for plagioclase measurements (geometric constructions, rotations, acquisition, etc.) were greatly simplified by an interactive program on a micro-computer (Benn & Mainprice 1989).

Plagioclase elastic constants used were determined by Aleksandrov *et al.* (1974). The symmetry of the velocity distribution is only monoclinic, as the constants were calculated assuming a monoclinic symmetry. The plagioclase in Fig. 5 (An_{56}) has a *P*-wave anisotropy of 35 per cent. We used data for anorthite contents of 56, 53 and 29 per cent (see Table 3) for our samples according to their anorthite percentage. In all cases, there is no symmetry difference; the highest *P*-wave velocity always corresponds to the **b** directions and the slowest to the **a*** crystallographic directions. The *S*-wave birefringence anisotropy pattern displays a complex topology with numerous maxima and minima with no simple relationship with the principal crystallographic axes. Only the **a** axis corresponds to the

Table 3. Single crystal seismic properties. The origin of the data used in this study and the main properties, such as the maximum and minimum *P*-wave velocity, the V_p anisotropy and the maximum birefringence of each crystal are indicated.

Single crystal elastic properties	Vpmax (Km/s)	Vpmin (Km/s)	Anis. (%)	ΔVs (Km/s)	References
plagioclase An56	8.0	5.6	29.6	1.3	Aleksandrov et al. (1974)
An53	7.8	5.7	27.4	1.3	"
An29	7.6	5.3	29.1	1.3	"
Clinopyroxene Augite	8.4	6.5	23.2	0.8	Aleksandrov et al. (1964)
Diopside	9.3	6.9	29.6	0.9	Levien et al. (1979)
Orthopyroxene Enstatite	8.2	7.3	11.3	0.5	Weidner et al. (1982)
Amphibole Hornblende	7.9	6.0	23.9	1.1	Aleksandrov and Ryzhova (1961)
Muscovite	8.2	4.6	44.3	2.7	Vaughan and Guggenheim (1986)
Olivine	9.9	7.7	21.8	0.9	Kumazawa and Anderson (1969)
Quartz (isotropic)	6.5	6.5	0.0	0.0	Kammer et al. (1948)
α-quartz (anisotropic)	6.3	4.9	23.3	1.50	Zubov et Firsova. (1962)
β-quartz (anisotropic)	6.6	6.4	3.3	0.66	"

minimum birefringence. The polarizations of the fast shear waves do not display simple trends.

5 3-D SEISMIC PROPERTIES OF THE SELECTED ROCKS

The seismic properties of the eight selected samples are presented in an equal area projection in Fig. 6. The 21 stiffness coefficients characterizing the elastic properties of these eight samples are presented in Table 4. In this section we will attempt to extract the most interesting features of these calculated seismic properties. The calculated results for the seismic velocities of each monomineralic aggregate (i.e. considering each mineral phase as a monomineralic rock) and for each whole rock are grouped in Table 5.

5.1 Pyroxenite 87VS28b

Clustering of clinopyroxene **b** axes in a maximum normal to the foliation causes a low V_p velocity normal to the foliation and a fast V_p within it. V_p anisotropy of the clinopyroxene aggregate (Table 5) is weak (4.1 per cent). On the other hand, orthopyroxene **b** axes are preferentially oriented within the foliation plane and should generate a slow *P*-wave velocity in the foliation plane. The orthopyroxene aggregate is nearly isotropic (V_p anisotropy 1.2 per cent) due to the weak fabric. When added together in proportion to the volumetric abundance, the whole rock becomes almost isotropic (1.8 per cent for the *P* waves). The fast velocity orientation of clinopyroxene corresponds to the slow velocity of the orthopyroxene and vice versa. Nevertheless, the stronger anisotropy of clinopyroxene controls the shape of the V_p distribution of the whole rock. Maximum V_p ($7.7\,km\,s^{-1}$) is oriented close to the Y structural axis whereas the minimum ($7.6\,km\,s^{-1}$) corresponds to the Z axis.

The *S*-wave birefringence pattern for this pyroxenite exhibits a complex pattern with a weak maximum ($0.08\,km\,s^{-1}$) oriented close to the lineation. *S* waves propagating along this direction are polarized with a fast shear wave parallel to the XZ structural plane.

5.2 Dunite 87VS148

This rock, composed of more than 95 per cent olivine, is the simplest possible case because it is almost monomineralic. Furthermore, olivine is orthorhombic and its preferred orientation also displays a well-developed orthorhombic symmetry. Calculated velocities display a previously described pattern (e.g. Christensen & Crosson 1968; Babuska 1972; Baker & Carter 1972; Carter, Baker & Georges' 1972; Peselnick, Nicolas & Stevenson 1974; Christensen & Salisbury 1979). The **a** axes preferred orientation close to the lineation causes high *P*-wave velocities ($9.0\,km\,s^{-1}$) close to the lineation for the aggregate. The strong **b** axis preferred orientation close to the foliation pole induces a low V_p velocity ($8.1\,km\,s^{-1}$) close to the pole of the foliation. This monomineralic rock displays high V_p anisotropy (9.7 per cent) due to the strong olivine preferred orientation and the absence of other mineral phases.

The shear wave birefringence pattern has a more complex topology, already described in other studies, calculated from LPOs (e.g. Mainprice & Silver 1993) or direct measurements (e.g. Kern 1993); the maximum ($0.3\,km\,s^{-1}$) is oriented close to the Y structural axis. The lineation (X axis) is almost isotropic to *S* waves because of the concentration of **a** axes parallel to X. The fast shear waves propagating along the directions of maximum splitting (i.e. parallel to Y) are polarized roughly parallel to the foliation plane. This simple example exhibits several typical features: (1) a monomineralic dunite, composed of an orthorhombic mineral with an orthorhombic preferred orientation symmetry, may generate a complex shear wave pattern and a complex birefringence pattern. The olivine single crystal pattern with two maxima of birefringence between the **a** and **c** axes is clearly responsible for this property. (2) Shear wave propagating along the X or Z structural axes are not expected to generate a big delay time. Only the Y structural axis (perpendicular to the lineation in the foliation plane) is a relatively highly birefringent ($0.25\,km\,s^{-1}$) direction. In this case the fast shear wave polarization plane is oriented parallel to the foliation plane.

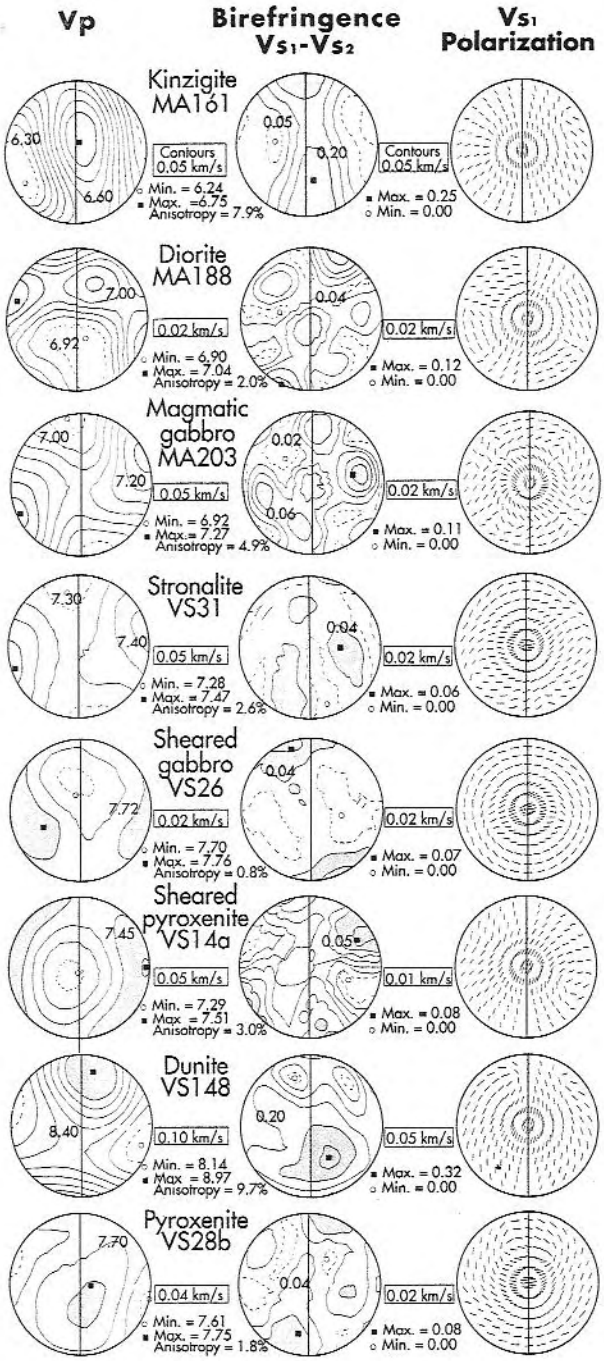

Figure 6. *P* and *S* seismic properties of the eight selected samples (equal area projection) in the structural frame (foliation N–S and lineation N–S). V_p spatial variations (left), *S*-wave birefringence ($V_{S_1} - S_{S_2}$) (middle) and polarization plane orientations of the fast shear wave (right) are displayed. The fastest velocity is located by a solid square and the lowest by an open circle. Note that the contour intervals are not the same for each sample. Shaded areas correspond to directions of high V_p or birefringence.

5.3 Sheared pyroxenite 87VS14a

The **c** axis preferred orientation nearly parallel to the lineation generates a high V_p in the clinopyroxene aggregate at 45° to the foliation. The minimum V_p is perpendicular to the lineation in the foliation plane. The weak and complex fabric produces a low *P*-wave anisotropy (4.1 per cent) for this clinopyroxene aggregate (Table 5). Plagioclase in this rock has an anorthite content of 56–58 per cent. The stiffness constants used were those measured for An_{56}. The V_p distribution in the plagioclase aggregate displays a weak anisotropy (4.4 per cent) with a $V_{P\max}$ normal to the foliation (corresponding to the **b** axis preferred orientation) and a $V_{P\min}$ close to the lineation (**a** axes concentration). These results compare fairly well with seismic properties of plagioclase aggregate determined in other studies (Ji & Mainprice 1988; Siegesmund *et al.* 1989). The resulting whole rock V_p anisotropy is weak (3.0 per cent) although the slow velocities of the two minerals (clinopyroxene and plagioclase) have similar orientations. Their summation has not been completely destructive. The anisotropy has been reduced by 10 per cent because isotropic garnet has replaced anisotropic materials. The overall velocity has been increased by this amount of garnet.

The *S*-wave birefringence pattern of this gabbro exhibits a very complex topology with several maxima and minima oriented at high angles to the main structural axes. The highest anisotropic direction of propagation (birefringence 0.08 km s^{-1}) is oriented at 45° of the X and Z axes and the lowest is close to the pole of the foliation. The fast shear wave polarization plane pattern also displays a complex geometry and has no systematic trend.

5.4 Sheared gabbro 87VS26

Plagioclase in this sample has an anorithite content of about 45–50 per cent. For calculations of seismic properties, the stiffness data determined for an anorthite content of An_{53} were used. The concentration of plagioclase **b** axes generates a high *P*-wave velocity oriented normal to the foliation of the aggregate. The **a** axes concentration oriented nearly parallel to the lineation generates a slow V_p direction close to the lineation. The relatively strong plagioclase LPO with a strong maximum results in a relatively high anisotropy (7.4 per cent) for the plagioclase aggregate. The clinopyroxene also displays a strong preferred orientation. The **c** axes oriented nearly parallel to the lineation produce a high V_p in this direction. The clinopyroxene **b** axes are oriented close to the pole of the foliation and generate a slow V_p normal to the foliation. For this clinopyroxene aggregate the anisotropy is high (8.2 per cent). The direction of high V_p in the clinopyroxene aggregate is similar to the direction of low V_p in the plagioclase aggregate. They have a destructive effect on anisotropy when summed together (see Fig. 7 (left) and Table 6). The orthopyroxene aggregate *P*-wave anisotropy is very weak (3.7 per cent). Summation of these three minerals in equivalent volume (Table 5) with 30 per cent isotropic garnet produces a nearly isotropic *P*-wave distribution for the whole rock (0.8 per cent anisotropy, $V_p = 7.7$ km s^{-1}). These results indicate that a stongly sheared mafic rock with strong fabric developed in granulitic conditions may have isotropic elastic properties.

This sample is also weakly anisotropic for the shear waves. The maximum birefringence (0.07 km s^{-1}) is oriented at a small angle to the lineation. The fast shear wave propagating along this direction is polarized parallel to the XZ plane. The minimum is oriented roughly normal to the foliation plane.

Table 4. Stiffness coefficients (in GPa) characterizing the elastic properties of the eight selected samples. The 21 C_{ij} were obtained combining LPOs of each constitutive mineral, single crystal stiffness constants, and rock modal compositions. These coefficients allow the calculation of the 3-D seismic velocities (P and S waves). The corresponding velocity contours are displayed in Fig. 6.

C_{ij} GPa	Pyroxenite 87VS28b	Dunite 87VS148	Sheared pyrox. 87VS14a	Sheared gabbro 87VS26	Stronalite 87VS31	Magmatic gabbro 87MA203	Diorite 87MA188	Kinzigite 87MA161
C_{11}	192.04	221.87	182.44	203.23	169.12	135.80	139.71	106.33
C_{22}	195.35	257.96	179.38	201.92	161.33	146.91	136.43	116.56
C_{33}	197.64	239.47	172.63	201.14	163.91	141.68	136.71	121.87
C_{44}	67.32	83.96	58.19	64.79	54.43	45.58	43.91	39.89
C_{55}	68.76	77.51	57.30	65.67	54.89	43.83	42.27	36.16
C_{66}	68.83	78.79	56.68	66.34	54.88	45.44	42.92	35.56
C_{12}	57.15	75.19	67.41	69.75	55.44	53.09	52.92	38.10
C_{13}	59.89	77.63	62.02	71.03	56.23	50.06	52.66	38.91
C_{14}	0.91	-1.03	0.14	-0.95	0.37	-0.04	0.94	0.06
C_{15}	0.00	-0.54	0.64	0.28	-0.26	0.15	0.15	1.22
C_{16}	1.21	3.68	-0.04	-0.18	1.10	-1.60	-1.28	-0.88
C_{23}	61.47	79.33	59.69	71.28	54.57	54.28	51.12	39.18
C_{24}	1.11	6.99	0.30	-0.16	-0.37	0.15	0.67	0.92
C_{25}	-0.17	0.35	1.72	0.09	0.31	0.16	-0.46	0.81
C_{26}	0.03	3.67	-1.01	0.17	0.57	-2.43	0.95	-1.36
C_{34}	-0.69	4.97	0.56	-0.46	-0.52	0.02	1.39	1.06
C_{35}	0.43	2.07	0.87	-0.25	0.31	0.65	0.16	1.58
C_{36}	0.53	2.08	-1.25	-0.17	-0.17	0.04	-0.31	-0.57
C_{45}	0.01	2.80	0.51	0.34	-0.08	0.57	0.53	-0.28
C_{46}	0.43	1.28	-0.15	0.11	0.31	0.00	0.21	1.23
C_{56}	-0.27	2.62	0.29	-0.07	0.34	-0.02	0.24	0.47

5.5 Stronalite 87VS31

Plagioclase (An_{40}) represents the major phase of this rock (45 per cent of the volume). The elastic constants of An_{29} were used. Plagioclase displays relatively strong LPO. The **b** axes are oriented close to the pole of the foliation and are responsible for the fast V_p normal to the foliation. Low P-wave velocities produced by the **a** axes concentration are oriented parallel to the lineation. Plagioclase aggregate displays a P-wave anisotropy of 9.2 per cent. The orthopyroxene aggregate is nearly isotropic (1.2 per cent) due to the poorly developed preferred orientation. Quartz in this sample (15 per cent of the rock) does not show strong fabric and was considered isotropic to facilitate calculations. The P-wave velocity distribution of the whole rock is qualitatively the same as the plagioclase (i.e. the same orientations of high V_p (7.5 km s^{-1}) near the Z axis and low V_p (7.3 km s^{-1}) near the lineation). The whole rock P-wave anisotropy coefficient has been reduced to 2.6 per cent. The 25 per cent of nearly isotropic orthopyroxene, 15 per cent isotropic garnet and 15 per cent isotropic quartz have a dramatic effect on the V_p anisotropy.

The sample 87VS31 has a complex shear wave birefringence pattern. The maximum birefringence is weak (0.06 km s^{-1}). Maximum and minimum birefringence are both oriented close to the lineation. This produces a relatively strong birefringence gradient close to the lineation; therefore, a small angular variation in the direction of propagation is expected to generate a large variation of birefringence introducing difficulties in the interpretation.

5.6 Magmatic gabbro 87MA203

Plagioclase measured in this sample has an anorthite content of about 65–70 per cent. The elastic stiffnesses of An_{56} were used. The fast V_p for this plagioclase aggregate is oriented normal to the foliation (due to the **b** axes concentrated close to the pole of the foliation) and the low V_p is oriented nearly parallel to the lineation (**a** axes concentration). The plagioclase aggregate is relatively anisotropic for the P waves (6.8 per cent). The orthopyroxene low V_p is perpendicular to the lineation within the foliation plane and the V_p distribution has an axial symmetry around this axis. Its anisotropy is weaker (5.0 per cent) than plagioclase. The V_p distribution for the whole rock is dominated by plagioclase (80 per cent of the volume). P waves propagate with a fast velocity (7.3 km s^{-1}) in a direction normal to the foliation and with a slow velocity (6.9 km s^{-1}) parallel to the lineation. The resulting V_p anisotropy is 4.9 per cent.

As described for the other gabbros, the shear wave birefringence pattern of this sample is more complex than the P-wave pattern. This is clearly caused by the complexity of the plagioclase single-crystal shear wave properties. In this rock, the high plagioclase content causes the whole rock maximum birefringence (0.11 km s^{-1}) to be oriented between the Z and Y structural axes. This kind of birefringence pattern has been already described in previous works (e.g. Siegesmund & Kruhl 1991). The foliation is a girdle of relatively high birefringence (>0.06 km s^{-1}). This rock displays strong birefringence variations, particularly for shear waves propagating at a high incidence angle to the foliation plane. The orientations of the fast S-wave polarization planes display a complex distribution without any simple trend or relationship to the structure.

5.7 Diorite 87MA188

The whole rock maximum and minimum V_p orientations are mainly controlled by the plagioclase (in the range An_{75-80}). This mineral phase is not strongly anisotropic (8.7 per cent) but represents a large volume (65 per cent) of the rock. The

Table 5. Anisotropic seismic properties of the eight selected rocks of the lower crustal section. The properties of each monomineralic aggregate and the whole rock properties are detailed. The maximum and minimum *P*- and *S*-wave velocities (and the V_p anisotropy) are given for each aggregate. Variations of the two shear waves (V_{S_1} and V_{S_2} as defined in the text) allow the determination of the birefringence ($V_{S_1} - V_{S_2}$).

			SEISMIC PROPERTIES							
SAMPLES	**Mineral**	**Mode (%)**	**Vp max (km/s)**	**Vp min (km/s)**	**Anisot. (%)**	**Vs_1 max (km/s)**	**Vs_1 min (km/s)**	**Vs_2 max (km/s)**	**Vs_2 min (km/s)**	**ΔVsmax (km/s)**
Pyroxenite	Cpx	50	7.4	7.1	4.1	4.3	4.2	4.2	4.1	0.10
87VS28b	Opx	50	8.0	7.9	1.2	4.8	4.8	4.8	4.7	0.08
	Whole Rock	100	7.7	7.6	1.8	4.6	4.5	4.5	4.5	0.08
Dunite	Olivine =	100	9.0	8.1	9.7	5.1	4.9	5.0	4.7	0.30
87VS148	**Whole Rock**									
Sheared	Plagioclase	25	7.0	6.7	4.4	3.8	3.6	3.7	3.6	0.30
pyroxenite	Cpx	65	7.4	7.1	4.1	4.3	4.2	4.2	4.1	0.10
87VS14a	Garnet	10	8.7	8.7	0.0	4.9	4.9	4.9	4.9	0.00
	Whole Rock	100	7.4	7.2	3.0	4.2	4.2	4.2	4.1	0.05
Sheared	Plagioclase	30	7.0	6.5	7.4	3.8	3.7	3.7	3.6	0.20
gabbro	Cpx	20	7.6	7.0	8.2	4.3	4.2	4.2	4.1	0.20
87VS26	Opx	20	8.1	7.8	3.7	4.8	4.8	4.8	4.7	0.10
	Garnet	30	8.7	8.7	0.0	4.9	4.9	4.9	4.9	0.00
	Whole Rock	100	7.7	7.7	0.8	4.4	4.4	4.4	4.4	0.00
Stronalite	Plagioclase	45	6.8	6.2	9.2	3.8	3.7	3.7	3.6	0.20
87VS31	Opx	25	8.0	7.9	1.2	4.8	4.8	4.8	4.7	0.06
	Quartz	15	6.5	6.5	0.0	4.0	4.0	4.0	4.0	0.00
	Garnet	15	8.7	8.7	0.0	4.9	4.9	4.9	4.9	0.00
	Whole Rock	100	7.5	7.3	2.6	4.3	4.2	4.3	4.2	0.80
Magmatic	Plagioclase	80	7.1	7.6	6.8	3.8	3.7	3.7	3.6	0.20
gabbro	Opx	20	6.1	5.8	5.0	3.3	3.2	3.3	3.2	0.10
87MA203	**Whole Rock**	100	7.3	6.9	4.9	4.1	3.9	4.0	3.9	0.10
Diorite	Plagioclase	65	7.2	6.6	8.7	3.8	3.6	3.7	3.6	0.20
87MA188	Cpx	8	8.3	7.6	8.8	4.6	4.4	4.5	4.3	0.30
	Opx	7	8.0	7.9	1.3	4.8	4.8	4.8	4.8	0.00
	Amphibole	10	7.2	6.6	8.7	3.9	3.7	3.8	3.6	0.20
	Biotite	10	7.2	5.8	21.5	4.3	3.7	3.8	3.6	0.70
	Whole Rock	100	7.0	6.9	2.0	3.9	3.8	3.9	3.8	0.10
Kinzigite	Plagioclase	55	6.6	6.3	4.6	3.7	3.5	3.6	3.5	0.30
87MA161	Quartz	25	6.5	6.5	0.0	4.0	4.0	4.0	4.0	0.00
	Biotite	20	7.7	5.2	38.8	4.6	3.4	3.7	3.4	1.20
	Whole Rock	100	6.8	6.3	7.9	3.9	3.7	3.8	3.6	0.30

four other mineral phases have a destructive influence on the anisotropy. $V_{p_{max}}$ in the plagioclase aggregate (normal to the foliation) corresponds to the orientation of the minimum velocities of the other minerals (augite, hornblende and biotite). Among the five minerals, only amphibole and biotite may have a constructive effect on V_p anisotropy when summed together (see Table 6); their slow and fast velocities have the same orientation (Fig. 7, right). This sample is the most complex of the eight selected rocks because of the five mineral phases. Although most of the mineral phases, except orthopyroxene, are relatively anisotropic (between 8 and 21 per cent), the bulk V_p anisotropy is very weak (2.0 per cent). Maximum and minimum V_p velocities of the various minerals are not similarly oriented. This induces a decrease in anisotropy when summed together. This rock illustrates the strong dependence of the number of minerals on the whole rock anisotropy.

The shear wave seismic properties of the sample 87MA188 also display a complex pattern. The maximum shear wave birefringence is weak ($0.12\,km\,s^{-1}$), but is oriented roughly parallel to the foliation. The polarization planes of the fast shear waves propagating in these directions of high birefringence are oriented parallel to the foliation.

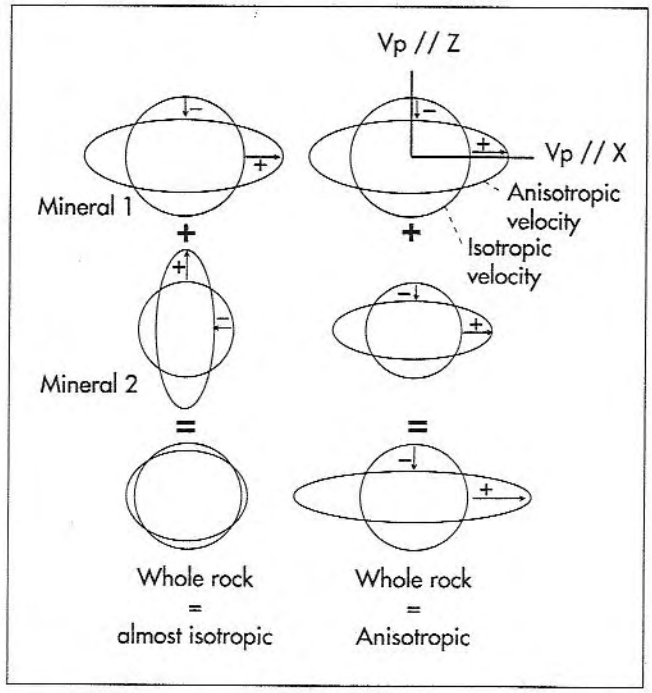

Figure 7. Seismic anisotropies of two mineral phases added together may enhance (right) or decrease (left) the resulting whole rock anisotropy, depending on the orientations of their fast and slow velocities compared to the isotropic property. The + and − correspond to the positive and negative variations of the aggregate compared to the isotropic case (see also Table 6 for real examples).

5.8 Kinzigite 87MA161

Plagioclase studied in this sample has a composition of An_{36-38}. The stiffness coefficients of An_{29} were used. Plagioclase in the sample has a well-organized petrofabric, resulting in a V_p anisotropy of 4.7 per cent for the monomineralic aggregate. *P* waves propagate at higher velocities in directions at a high angle to the foliation and slower in directions nearly parallel to the lineation. Biotite has a strong preferred orientation causing an extremely high V_p anisotropy (38 per cent) for the biotite aggregate. Poles of the (001) planes are well concentrated around the pole of the foliation. *P* waves propagate quickly within the foliation plane and velocity decreases steeply when the propagation direction becomes closer to the pole of the foliation. The quartz LPO is poorly organized. Only the **c** axis orientation was determined and this does not permit calculations of seismic properties. For these two reasons, we assumed a random orientation of quartz, as described previously. *P*-wave velocity distribution for the whole rock is clearly controlled by biotite. This mineral represents a significant volume of the rock (20 per cent). The axial symmetry around the pole of the foliation created by the biotite is clearly the most important feature of the whole rock seismic property. The directions of high V_p (6.7 km s^{-1}) are parallel to the foliation plane, whereas the low V_p (6.3 km s^{-1}) are at a high angle with it. The resulting V_p anisotropy is relatively strong (7.9 per cent). Biotite, even in relatively small volumes, may strongly influence rock anisotropy. Several authors have made similar observations, either by direct laboratory measurement or by calculations from LPOs (e.g. Christensen 1965; Fountain, Hurich & Smithson 1984; Kern & Wenk 1990; Burlini & Fountain 1993).

The shear wave birefringence pattern of this metapelite displays the same symmetry as the *P*-wave pattern, and is also clearly controlled by the high content of phyllosilicate minerals. The rock birefringence displays an axial symmetry around the pole of the foliation because of the biotite preferred orientation. The maximum birefringence is strong (0.25 km s^{-1}) and oriented parallel to the lineation, but the most interesting feature is that the birefringence is systematically higher than 0.20 km s^{-1} for waves propagating parallel to the foliation. Shear waves propagating at high incidence angles to the foliation do not split, whereas waves propagating parallel to the foliation plane strongly split, and the fast shear wave is polarized parallel to the XY plane (i.e. the foliation plane). This birefringence pattern is in complete agreement with direct laboratory measurements (e.g. Christensen 1966) and with other calculations (e.g. Burlini & Fountain 1993). The correlations between seismic properties and tectonic fabric have already been found by other authors (e.g. Kern, Schmidt & Popp 1991).

Table 6. Anisotropic seismic properties of the six major mineral phases with typical crystallographic preferred orientations found in this work. The increase or decrease (+ or − respectively) of *P*-wave velocities compared to the isotropic case were calculated for each structural axis (X = lineation, Y, Z = pole of the foliation). Only the calculated birefringence along each structural axis is reported for the shear waves. For a given direction, two mineral phases with identical signs (+ or −) added together will enhance the anisotropy (see also Fig. 7).

Typical mineral LPO	Vp mean (km/s)	X ΔVp (km/s)	X birefr (km/s)	Y ΔVp (km/s)	Y birefr (km/s)	Z ΔVp (km/s)	Z birefr (km/s)
Biotite (MA161)	6.70	+ 0.92	1.10	+ 0.64	1.15	- 1.46	0.08
Amphibole (MA188)	6.92	+ 0.11	0.20	+ 0.08	0.21	- 0.27	0.09
Plagioclase (VS26)	6.74	- 0.21	0.09	- 0.07	0.11	+ 0.22	0.02
Opx (VS26)	7.93	- 0.04	0.04	- 0.10	0.01	+ 0.10	0.03
Cpx (VS26)	7.36	+ 0.14	0.19	- 0.02	0.09	- 0.35	0.14
Olivine (VS148)	8.50	+ 0.33	0.17	+ 0.01	0.25	- 0.34	0.17

6 DISCUSSION

6.1 What controls the intrinsic anisotropy?

Rock *P*-wave anisotropies calculated in this study range from 1 to 10 per cent. The anisotropy is a function of the single crystal properties, the LPO of each mineral and the rock composition (nature, number and relative proportions of mineral phases).

The properties of the single crystal, through its intrinsic anisotropy and its symmetry, is the first factor controlling the anisotropy. For a given LPO the result will be less anisotropic if the single crystal properties are less anisotropic. This factor is obvious in monomineralic rocks but some strongly anisotropic minerals, such as biotite and more generally phyllosilicates, even in small fractions (i.e.

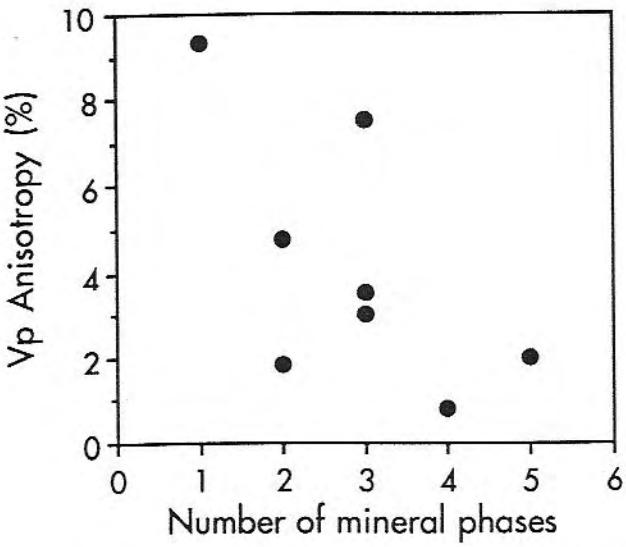

Figure 8. Influence of the number of mineral constituents of a rock on its seismic anisotropy. The calculated V_p anisotropy for the eight samples versus the number of their constituent mineral phases is plotted. Monomineralic rocks are clearly the most anisotropic whereas complex rocks are nearly isotropic.

<20 per cent by volume), may strongly influence the whole rock anisotropy (e.g. Barruol *et al.* 1992; Barruol & Mainprice 1993). For example, the seismic properties of the kinzigite 87–MA161 are strongly influenced by biotite, although it represents only 20 per cent of the rock.

The intensity of crystallographic preferred orientations also controls the resulting anisotropy of a monomineralic aggregate. If one considers a monomineralic rock (the dunite 87VS148, for instance), the total anisotropy is between an isotropic end member (a situation where crystals are randomly oriented) and a situation of maximum anisotropy (if all grains have the same orientation) corresponding to the single crystal anisotropy (24 per cent for *P* waves in olivine). Anisotropy between these two theoretical end members is only a function of the fabric intensity.

Finally, the main factor controlling the whole rock anisotropy is the number of constitutive elements of the rock. The anisotropy steeply decreases when the number of constitutent minerals increases (Fig. 8). The gabbro 87VS26 is a typical example of a strongly sheared rock with a well-developed fabric that displays almost isotropic seismic properties. Each mineral phase (i.e. plagioclase and pyroxene) develops relatively strong preferred orientations. Their respective *P*-wave anisotropies (7.4 and 8.2 per cent) are significant. As a result, when these two mineral phases are added together (Fig. 7, left), the whole rock becomes nearly isotropic (0.8 per cent). The plagioclase maximum *P*-wave velocity orientation corresponds to the clinopyroxene minimum velocity orientation and vice versa.

To quantify the influence of each mineral phase encountered in the studied lower crustal section, and particularly the effect they may induce on anisotropy when added together, the anisotropic seismic properties of six typical monomineralic aggregates with typical LPOs are summarized in Table 6. For each mineral, a typical fabric is selected among all the measurements performed in this work and its anisotropic seismic properties are determined. The anisotropic *P*-wave velocities along each structural axis are compared to the isotropic case. The biotite aggregate for instance has very high V_p along the X and Y directions (respectively +0.92 and +0.64 km s^{-1} compared to the isotropic velocity), whereas V_p in the Z direction is 1.46 km s^{-1} lower than the isotropic velocity (6.70 km s^{-1}). Birefringence is also very high along the X and Y direction and very weak parallel to the Z direction. Table 6 displays relationships between the orientation of the fast and slow V_p and the structural reference frame. It allows one to see if the the co-existence of two or more mineral phases will enhance or decrease the resulting seismic anisotropy. For a given structural direction, two positive V_p added together increase the resulting anisotropy (Fig. 7, right). From the selected crystallographic preferred orientations, it may be concluded that very few minerals display a constructive effect simultaneously in the three structural directions when added together. The biotite and amphibole combination is the most efficient coupling possible because both minerals are very anisotropic and have similar velocity symmetries. This may occur for instance in paragneisses or amphibolites. Olivine also displays the same characteristics but is not frequently associated with amphibole and biotite in natural situations. Plagioclase and orthopyroxene also have similar anisotropy orientations, but orthopyroxene is weakly anisotropic. These considerations explain why, from a statistical point of view, the *P*-wave anisotropy decreases when the number of constituent increases (cf. Fig. 8). For the shear waves, it is more complicated to predict the effect of several mineral phases added together because not only does the velocity difference play a role, but also the orientations of the polarization planes have an important influence.

6.2 Role of anisotropy on the lower crustal seismic reflectivity

From the *P*-wave velocities of the eight representative lower crustal lithologies, the reflection coefficients for all possible lithological interfaces are calculated. The results are summarized in Table 7. The foliation is assumed to be horizontal and seismic wave propagating at near-vertical incidence. This kind of geometry should correspond to the study of a horizontally 'layered lower crust' using near-vertical seismic reflections. The reflection coefficients (RCs) are calculated first using the *P*-wave velocity normal to the foliation in the anisotropic case (Table 7a) and then using the isotropic velocities (Table 7b). The calculation of the isotropic velocity from the 21 elastic constants has been done using the Voigt average. For the anisotropic case, about 50 per cent of the possible interfaces generate RCs lower than 0.10, and about 30 per cent lower than 0.05. About 50 per cent of the interfaces generate RCs higher than 0.10. Not all of these interfaces physically exist in the Val Sesia area but they may be found in other sections of the lower crust and crust to mantle transition.

From two particular examples of interfaces, we can see that the anisotropy may either enhance or decrease the

Table 7. Reflection coefficient (RC) amplitudes calculated at each possible interface between the eight representative lower crustal rocks. The *P*-wave propagation is assumed to be at near-vertical incidence and the foliation horizontal. The density and velocity of each rock are given. The RCs were first calculated using the velocity of the anisotropic case (Table 7a) and then using the isotropic velocities (Table 7b). The residual between the two RCs are shown in Table 7(c). It allows us to quantify the influence of the anisotropy on the RC amplitudes.

(a) RC amplitudes considering the vertical velocities for the *anisotropic* medium

Sample Upper / Lower	Density	V_p anis.	Pyroxenite	Dunite	Sheared pyroxenite	Sheared gabbro	Stronalite	Magmatic gabbro	Diorite	Kinzigite
			3.30	3.31	3.24	3.38	3.04	2.82	2.84	2.70
			7.60	8.50	7.50	7.76	7.45	7.20	7.02	6.30
Pyroxenite	3.30	7.60	—	0.06	-0.02	0.02	-0.05	-0.10	-0.11	-0.19
Dunite	3.31	8.50	-0.06	—	-0.07	-0.04	-0.11	-0.16	-0.17	-0.25
Sheared pyroxenite	3.24	7.50	0.02	0.07	—	0.04	-0.04	-0.09	-0.10	-0.18
Sheared gabbro	3.38	7.76	-0.02	0.04	-0.04	—	-0.07	-0.13	-0.14	-0.21
Stronalite	3.04	7.45	0.05	0.11	0.04	0.07	—	-0.05	-0.06	-0.14
Magmatic gabbro	2.82	7.20	0.10	0.16	0.09	0.13	0.05	—	-0.01	-0.09
Diorite	2.84	7.02	0.11	0.17	0.10	0.14	0.06	0.01	—	-0.08
Kinzigite	2.70	6.30	0.19	0.25	0.18	0.21	0.14	0.09	0.08	—

(b) RC amplitudes considering the vertical velocities for the *isotropic* medium

Sample Upper / Lower	Density	V_p iso.	Pyroxenite	Dunite	Sheared pyroxenite	Sheared gabbro	Stronalite	Magmatic gabbro	Diorite	Kinzigite
			3.30	3.31	3.24	3.38	3.04	2.82	2.84	2.70
			7.70	8.10	7.41	7.73	7.36	7.09	6.97	6.51
Pyroxenite	3.30	7.70	—	0.03	-0.03	0.01	-0.06	-0.12	-0.12	-0.18
Dunite	3.31	8.10	-0.03	—	-0.06	-0.01	-0.09	-0.15	-0.15	-0.21
Sheared pyroxenite	3.24	7.41	0.03	0.06	—	0.04	-0.04	-0.09	-0.10	-0.16
Sheared gabbro	3.38	7.73	-0.01	0.01	-0.04	—	-0.08	-0.13	-0.14	-0.20
Stronalite	3.04	7.36	0.06	0.09	0.04	0.08	—	-0.06	-0.06	-0.12
Magmatic gabbro	2.82	7.09	0.12	0.15	0.09	0.13	0.06	—	-0.01	-0.07
Diorite	2.84	6.97	0.12	0.15	0.10	0.14	0.06	0.01	—	-0.06
Kinzigite	2.70	6.51	0.18	0.21	0.16	0.20	0.12	0.07	0.06	—

(c) Residuals | RC Aniso.| - | RC Iso.|

Sample upper / Lower	Pyroxenite	Dunite	Sheared pyroxenite	Sheared gabbro	Stronalite	Magmatic gabbro	Diorite	Kinzigite
Pyroxenite	—	0.031	0.013	0.008	0.013	0.014	0.010	-0.010
Dunite	-0.031	—	-0.018	-0.022	-0.018	-0.016	-0.020	-0.038
Sheared pyroxenite	-0.013	0.018	—	-0.004	0.000	0.002	-0.002	-0.022
Sheared gabbro	-0.008	0.022	0.004	—	0.004	0.006	0.002	-0.018
Stronalite	-0.013	0.018	0.000	-0.004	—	0.002	-0.002	-0.022
Magmatic gabbro	-0.014	0.016	-0.002	-0.006	-0.002	—	-0.004	-0.024
Diorite	-0.010	0.020	0.002	-0.002	0.002	0.004	—	-0.020
Kinzigite	0.010	0.038	0.022	0.018	0.022	0.024	0.020	—

magnitude of the RC.

(1) The kinzigite/magmatic gabbro interface has an RC of 0.09 for the anisotropic case, whereas this value decreases to 0.07 for the isotropic case (in absolute values). The anisotropy therefore enhances the reflection coefficient. This is explained by the fact the wave propagates parallel to the minimum velocity in the upper medium and parallel to the maximum velocity in the lower one. In the isotropic case the velocity is enhanced in the upper medium and decreased in the lower one. The velocity contrast and, hence, the acoustic impedance are lowered, causing a decrease of the reflection coefficient magnitude.

(2) On the other hand, the sheared pyroxenite/pyroxenite interface illustrates the opposite effect. The reflection coefficient is lower in the anisotropic case (0.02) than in the isotropic one (0.03). In this example, the anisotropy clearly plays a destructive role although the absolute values are low.

In Table 7(c) we summarize the systematic variations of the RC amplitude between the anisotropic and the isotropic case. At each given interface we determined a 'residual' reflection coefficient which is defined as the difference between the anisotropic and the isotropic RC (in absolute values). Results are plotted in Fig. 9. Although the number of interfaces is relatively small, we observe several features: (1) an asymmetric distribution between −0.02 and 0.04 not centred at the zero value. This indicates the RCs are not insensitive to the anisotropy. From a statistical point of view, RC magnitudes are slightly enhanced when rocks are considered to be anisotropic. (2) About 50 per cent of the residuals are lower than 0.01 (absolute values). This means that the considered lithological interfaces are not sensitive to the anisotropy. (3) Few interfaces (10 per cent) are significantly less reflective (i.e. RC lowered more than 0.01) when one considers the anisotropic properties. (4) On the other hand, 40 per cent of the interfaces are significantly more reflective (RC enhanced of more than 0.01) in the anisotropic cases.

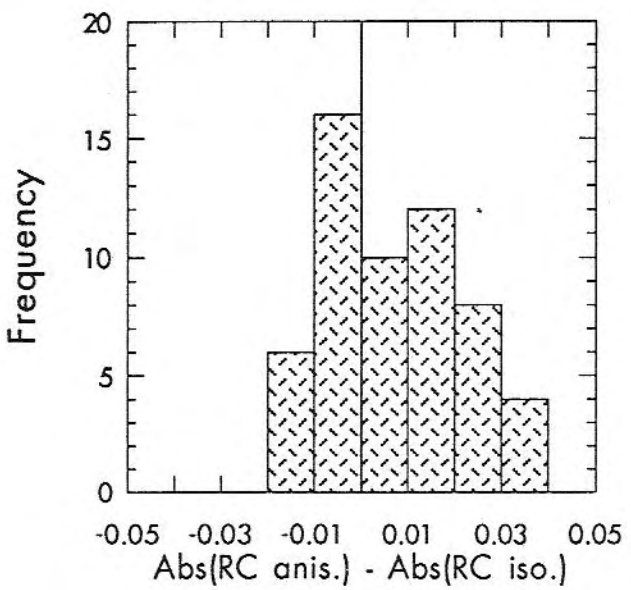

Figure 9. Frequency histogram of the reflection coefficient on the whole range of possible lithologic interfaces between the anisotropic case and the isotropic case. This 'residual' coefficient is calculated as the difference between the absolute value of the anisotropic reflection coefficient (Table 7a) and the isotropic coefficient (Table 7b). This distribution is not symmetrical around the zero value (i.e. the anisotropy plays a role on the reflection coefficients). The anisotropy enhances the reflection coefficient (versus the isotropic case) for 60 per cent of interfaces. See text for more details.

The crust–mantle transition in the Val Sèsia section, as presented in Fig. 2 and rotated in its assumed initial orientation, is characterized by numerous *P*-wave reflections of relatively high magnitudes (up to 0.10). The mafic body is seismically transparent whereas the reflection at the contact kinzigite-diorite or kinzigite gabbro is relatively strong (in the range 0.06–0.09). This reflectivity profile compares fairly well with results of Burke & Fountain (1990). This crust–mantle transition could be a good example of a geophysical Moho, characterized by a zone of transitional velocities between typical crustal values and mantle velocities (Hale & Thompson 1982). This Moho is not a first-order discontinuity but a laminated transition zone. As shown by Fountain (1989), material underplatted at the bottom of the crust may strongly influence the reflection characteristics of the lower crust and of the Moho discontinuity.

7 CONCLUSIONS

In this study, we determined the complete 3-D seismic properties of eight representative samples from a section through the lower crust and the crust–mantle transition. Their 21 stiffness constants were calculated using their lattice preferred orientations and the stiffness coefficients of the single crystals. We draw the following conclusions:

(1) Petrofabric measurements allow the determination of the true 3-D seismic properties (the 21 stiffness coefficients) of complex rocks.

(2) We can better define the relative influence of single crystal properties, preferred orientation of each mineral and modal composition of the rock on the final resulting seismic properties.

(3) In this mafic lower crust, *P*-wave anisotropy is typically in the range 2–5 per cent and is strongly influenced by the number of minerals in the rock. Monomineralic rocks have the highest anisotropy (10 per cent for the monomineralic dunite) whereas polymineralic rocks are weakly anisotropic (<3 per cent).

(4) Phyllosilicates strongly influence the *P*- and *S*-wave anisotropies and the axial symmetry of their preferred orientations often results in an axial symmetry of the seismic properties.

(5) Calculated *S*-wave birefringences are in the range 0.0–0.3 km s^{-1} and display complex patterns. Mafic rocks, such as pyroxenites or pyroxene-rich gabbros, are weakly anisotropic: their shear wave birefringence is systematically lower than 0.1 km s^{-1}. They are not good candidates for strong lower crustal *S*-wave splitting. Their birefringence patterns have very complex topologies, the orientations of their maximum birefringences do not display a direct relationship with the structural frame, and their polarization planes also display complex orientations. On the other

hand, olivine-rich rocks such as dunite, have relatively strong *S*-wave birefringence with a maximum ($0.3\,km\,s^{-1}$) oriented perpendicularly to the lineation within the foliation plane. The fast split shear waves propagating in these highly birefringent directions are polarized parallel to the foliation plane.

(6) Felsic rocks, such as biotite-bearing gneisses, display significant anisotropy (birefringence $0.30\,km\,s^{-1}$). Polarization planes of the fast split shear waves are clearly related to the tectonic fabric. Maximum birefringence corresponds to the foliation plane and the fast split shear wave propagating parallel to the foliation systematically polarizes parallel to it.

(7) We determined the influence of several typical LPOs found in samples from this lower crustal section on the resulting anisotropy. Only phyllosilicates and amphiboles clearly enhance the V_p anisotropy when added together. Summation of other mineral phases with the measured LPOs systematically decreases the anisotropy.

(8) Considering 56 possible lithologic interfaces, we analysed the real influence of the anisotropy (compared to the isotropic case) on the reflection coefficient. The anisotropy has a complex and unsystematic influence on the reflectivity. Compared to the isotropic case, anisotropy tends to enhance the reflection coefficient for 60 per cent interfaces (by values up to 0.03) but at 40 per cent of the interfaces, it lowers the reflection coefficient magnitudes.

(9) The reflection profile of the Val Sesia section, in its assumed horizonatal orientation, is characterized by a laminated crust to mantle transition that displays reflections of relatively high amplitude (up to 0.10). This study supports the interpretation that bright Moho reflections observed in extended terranes might be attributed to underplatting of magmas.

ACKNOWLEDGMENTS

This study has been supported by the Accompagnement ECORS 90/91 N°891706, by the DBT program Thème Géodynamique and by the ATP Thème Tomographie. Thanks are due to F. Boudier and P. Munch for their useful help and discussion in the field. We are also thankful to D. Fountain and an anonymous reviewer for constructive comments, and to A. Vauchez for this helpful discussions.

REFERENCES

Aleksandrov, K. S. & Ryzhova, T. V., 1961. The elastic properties of rock forming minerals II: Layered silicates, *Izv. Acad. Sci. USSR, Geophys. Phys. Solid Earth*, 1165–1168.

Aleksandrov, K. S., Ryzhova, T. V. & Belikov, B. P., 1964. The elastic properties of pyroxenes, *Sov. Phys. Crystllogr.*, **8,** 589–591.

Aleksandrov, K. S., Alchikov, U. V., Belikov, B. P., Zaslavskii, B. I. & Krupnyi, A. I., 1974. Velocities of elastic waves in minerals at atmospheric pressure and increasing precision of elastic constants by means of EVM (in Russian), *Izv. Acad. Sci. USSR, Geol. Ser.*, **10,** 15–24.

Allard, B. & Sotin, C., 1988. Determination of mineral phase percentages in granular rocks by image analysis on a microcomputer, *Comput. Geosci.*, **14,** 261–269.

Babuska, V., 1972. Elasticity and anisotropy of dunite and bronzite, *J. geophys. Res.*, **77,** 6955–6965.

Barruol, G., 1993. Anisotropies sismiques dans la croûte inférieure, *Thèse de doctorat*, Université de Montpellier II.

Barruol, G. & Kern, H., 1993. *P* and *S* waves velocities and shear wave splitting in the lower crustal/upper mantle transition (Ivrea Zone). Experimental and calculated data, *Geophys. J. Int.*, submitted.

Barruol, G. & Mainprice, D., 1993. A quantitative evaluation of the contribution of crustal rocks to the shear wave splitting of teleseismic SKS waves, *Phys. Earth planet. Inter.*, **78,** 281–300.

Barruol, G., Mainprice, D. Kern, H., Saint Blanquat, M. & Compte, P., 1992. 3D seismic study of a ductile shear zone from laboratory and petrofabric data (Saint Barthélémy Massif, Northern Pyrénées, France), *Terra Nova*, **4,** 63–76.

Baker, D. W. & Carter, N. L., 1972. Seismic velocity anisotropy calculated for ultramafic minerals and aggregates, in *Flow and fracture of rocks*, pp. 157–166, eds Heard, H. C., Borg, I. Y., Carter, N. L. & Raleigh, C. B., Am. geophys. Un., Washington, DC.

Bayer, R., Carozzo, M. T., Lanza, R., Miletto, M. & Rey, D., 1989. Gravity modelling along the ECORS-CROP vertical seismic reflection profile through the western Alps, *Tectonophysics*, **162,** 203–218.

Benn, K. & Mainprice, D., 1989. An interactive program for determination of plagioclase crystal axes orientations from U-stage measurements: an aid for petrofabric study, *Comput. Geosci.*, **15,** 1127–1142.

Berckemer, H., 1968. Topographie des 'Ivrea körper' abgeleitet aus seismichen und gravimetrischen daten, *Schweiz. Mineral. Petrogr. Mitt.*, **48,** 235–284.

Boriani, A., Burlini, L. & Sacchi, R., 1990. The Cossato–Mergozzo–Brissago line and the Pogallo line (Southern Alps, Northern Italy) and their relationships with the late hercynian magmatic and metamorphic processes, *Tectonophysics*, **182,** 91–102.

Boudier, F., Jackson, M. & Nicolas, A., 1984. Structural study of the Balmuccia massif (western Alps): A transition from mantle to lower crust, *Geologie en Mijnbouw*, **16,** 179–188.

Brodie, K. H. & Rutter, E. H., 1987. Deep crustal extensional faulting in the Ivrea Zone of northern Italy, *Tectonophysics*, **140,** 93–212.

Brodie, K. H., Rex, D. & Rutter, E. H., 1989. On the age of deep crustal faulting in the Ivrea zone, northern Italy, in *Alpine, Tectonics*, pp. 203–210, eds. Coward M. P., Dietrich, D. & Park, R. G., Geological Society Special Publication.

Brodie, K. H., Rutter, E. H. & Evans, P., 1992. On the structure of the Ivrea–Verbano zone (Northern Italy) and is implication for present-day lower continental crust geometry, *Terra Nova*, **4,** 34–40.

Burke, M. M. & Fountain, D. M., 1990. Seismic properties of rocks exposure of extended continental crust—new laboratory measurements from the Ivrea zone, *Tectonophysics*, **182,** 119–146.

Burlini, L. & Fountain, D. M., 1993. Seismic anisotropy of metapelites from the Ivrea–Verbano zone and Serie dei Laghi (N. Italy), *Phys. Earth planet. Inter.*, **78,** 301–317.

Burri, C., Parker, R. L. & Wenk, E., 1967. *Die optische orientierung der plagioklase*, Birkhäser, Basel.

Carter, N. L., Baker, D. W. & Georges, R. P., 1972. Seismic anisotropy, flow and constitution of the upper mantle, in *Flow and fracture of rocks*, pp. 167–190, eds Heard, H. C., Borg, I. Y., Carter, N. L. & Raleigh, C. B., Am. geophys. Un., Washington, DC.

Christensen, N. I., 1965. Compressional wave velocities in metamorphic rocks at pressures to 10 kilobars, *J. geophys. Res.*, **70,** 6147–6164.

Christensen, N. I., 1966. Shear wave velocities in metamorphic rocks at pressures to 10 kilobars, *J. geophys. Res.*, **71,** 3549–3556.

Christensen, N. I. & Crosson, R. S., 1968. Seismic anisotropy in the upper mantle, *Tectonophysics*, **6,** 93–107.

Christenssen, N. I. & Salisbury, M. H., 1979. Seismic anisotropy in the oceanic upper mantle: evidence from the bay of Island ophiolite complex, *J. geophys. Res.*, **84,** 4601–4610.

Crosson, R. S. & Lin, J. W., 1971. Voigt and Reuss prediction of anisotropic elasticity of dunite, *J. geophys. Res.*, **76,** 570–578.

Cumming, G. L., Köppel, V. & Ferrario, A., 1987. A lead isotopes study of the northeastern Ivrea Zone and the adjoining Ceneri Zone (N-Italy): evidence for a contaminated subcontinental mantle, *Contr. Miner. Petrol.*, **97,** 19–30.

Fountain, D. M., 1976. The Ivrea-Verbano and Strona–Ceneri Zones, northern Italy: A cross-section of the continental crust—new evidence from seismic velocities of rock samples, *Tectonophysics,* **33,** 145–165.

Fountain, D. M., 1986. Implication of deep crustal evolution for seismic interpretation, in *Reflection Seismology: The Continental Crust,* pp. 1–7, eds Barazangi, M., & Brown, L., Am. Geophys. Un., Washington, DC.

Fountain, D. M., 1989. Growth and modification of lower continential crust in extended terrains: the role of extension and magmatic underplating, in *Properties and Processes of Earth's Lower Crust,* pp. 287–299, eds Mereu, R. F., Mueller, S. & Fountain, D. M., Am. geophys. Un., Washington, DC.

Fountain, D. M. & Salisbury, M. H., 1981. Exposed cross-sections through the continental crust: Implication for crustal structure, petrology and evolution, *Earth planet. Sci. Lett.*, **56,** 263–277.

Fountain, D. M., Hurich, C. A. & Smithson, S. B., 1984. Seismic reflectivity of mylonite zones in the crust, *Geology,* **12,** 195–198.

Furlong, K. P. & Fountain, D. M., 1986. Continental crust underplatting: thermal considerations and seismic–petrologic consequences, *J. geophys. Res.*, **91,** 8285–8294.

Giese, P., 1968. Die strucktur der erdkruste im bereich der Ivrea Zone, *Schweiz. Mineral. Petrogr. Mitt.*, **48,** 261–284.

Hale, L. D. & Thompson, G. A., 1982. The seismic reflection character of the continental mohorovicic discontinuity, *J. geophys. Res.*, **87,** 4625–4635.

Handy, M., 1987. The structure, age and kinematics of the Pogallo fault zone; southern Alps, northern Italy, *Eclogae Geol. Helv.*, **3,** 593–632.

Hodges, K.V. & Fountain, D. M., 1984. Pogallo line, south Alps, northern Italy: An intermediate crustal level, low-angle normal fault?, *Geology,* **12,** 151–155.

Hunziker, J. C. & Zingg, A., 1980. Lower paleozoic amphibolite to granulite facies metamorphism in the Ivrea Zone (southern Alps, Northern Italy), *Schweiz. Mineral. Petrogr. Mitt.*, **60,** 181–213.

Hurich, C. A. & Smithson, S. B., 1987. compositional variation and the origin of deep crustal reflections, *Earth planet. Sci. Lett.*, **85,** 416–426.

H. S. & Mainprice, D., 1988. Natural deformation fabrics of plagioclases: implications for slip systems and seismic anisotropy, *Tectonphysics,* **147,** 145–163.

Kälin, O. & Trümpy, D., 1977. Sedimentation und paläotektonik in den westlichen Südalpen: Zur triadisch-jurassischen Gesichte der Monte Nudo-Beckens, *Eclogae Geol. Helv.*, **70,** 295–350.

Kammer, E. W., Pardue, T. E. & Frissel, H. F., 1948. A determination of the elastic constants for beta-quartz, *J. appl. Phys.*, **19,** 265–270.

Kern, H., 1993. *P*- and *S*-wave anisotropy and shear wave splitting at pressure and temperature in possible mantle rocks and their relations to the rock fabric, *Phys. Earth planet. Inter.*, **78,** 245–256.

Kern, H. & Wenk, H. R., 1990., Fabric-related velocity anisotropy and shear wave splitting in rocks from Santa Rosa mylonite zone, California, *J. geophys. Res.*, **95,** 11 213–11 223.

Kern, H., Schmidt, R. & Popp, T., 1991. The velocity and density structure of the 4000 m crustal segment at the KTB drilling site and their relationship to lithological and microstructural characteristics of the rocks: an experimental approach, *Sci. Drill.*, **2,** 130–145.

Köppel, V., 1974. Isotopic U–Pb ages of monazites and zircons from the crust–mantle transition and adjacent units of the Ivrea and Ceneri Zones (southern Alps, Italy), *Contr. Miner. Petrol.*, **43,** 55–70.

Kumazawa, M. & Anderson, O. L., 1969. Elastic moduli, pressure derivatives and temperature derivatives of single crystal olivine and single crystal forsterite, *J. geophys. Res.*, **74,** 5961–5980.

Levien, L., Weidner, D. J. & Prewitt, C. T., 1979. Elasticity of diopside, *Phys. Chem. Miner.*, **4,** 105–113.

Mainprice, D., 1990. A FORTRAN program to calculate seismic anisotropy from the lattice preferred orientation of minerals, *Comput. Geosci.*, **16,** 385–393.

Mainprice, D. & Silver, P. G., 1993. Constraints on the interpretation of teleseismic SKS observations from kimberlites nodules from the subcontinental mantle, *Phys. Earth planet. Inter.*, **78,** 257–280.

Mainprice, D., Casey, M. & Schmid, S., 1990a. The seismic properties of Alpine quartz and calcite mylonites determined from the orientation distribution function, *Mém. Soc. géol. France,* **156,** 85–95.

Mainprice, D., Humbert, M. & Wagner, F., 1990b. Phase transformations and inherited lattice preferred orientation: Implications for seismic properties, *Tectonophysics,* **180,** 213–228.

Nicolas, A., 1984. Lherzolites of western Alps: a structural review, in *Kimberlites II: The Mantle and Crust–Mantle Relationships,* pp. 333–345, ed. Kornprobst, J., Elsevier, Amsterdam.

Nicolas, A., Polino, R., Hirn, A., Nicolich, R. & ECORS-CROP-team, 1990. ECORS-CROP traverse and deep structure of the western Alps: a synthesis, *Mém. Soc. géol. France,* **156,** 15–27.

Peselnick, L., Nicolas, A. & Stevenson, P. R., 1974. Velocity anistropy in a mantle periodotite from the Ivrea Zone: Application to upper mantle anisotropy, *J. geophys. Res.*, **79,** 1175–1182.

Pin, C., 1986. Datation U–Pb sur zircons à 285 Ma du complexe gabbro–dioritique du Val Sesia–Val Mastallone et âge tardi-hercynien du metamorphisme granulitique de la zone Ivrea–Verbano (Italie), *C. R. Acad. Sci., Paris,* **9,** 827–830.

Pin, C. & Sills, J. D., 1986. Petrogenesis of layered gabbros and ultramafic rocks from Val Sesia, NW Italy: trace elements and isotope geochemistry, in *The Nature of the Continental Crust,* pp. 231–249, eds Dawson, J. B., Carswell, D. A., Hall, J. & Wedepohl, K. H., London.

Quick, J. E., Sinigoi, S., Negrini, L., Demarchi, G. & Mayer, A., 1992. Synmagmatic deformation in the underplated igneous complex of the Ivrea–Verbano zone, *Geology,* **20,** 613–616.

Rey, D., 1989. Structure crustale des Alpes occidentales le long du profil ECORS-CROP d'après la sismique reflexion et le champ de pesanteur, *Thèse de Doctorat,* Montpellier II.

Rivalenti, G., Garutti, G., Rossi, A., Siena, F. & Sinigoi, S., 1981. Existence of different peridotite types and of a layered igneous complex in the Ivrea Zone of the western Alps, *J. Petrol.*, **22,** 127–153.

Schmid, R. & Wood, B. J., 1976. Phase relationships in granulitic metapelites from the Ivrea–Verbano Zone (Northern Italy), *Contr. Mineral. Petrol.*, **54,** 255–279.

Schmid, S. M., Zingg, A. & Handy, M., 1987. The kinematics of movements along the Insubric Line and the emplacement of the Ivrea Zone, *Tectonophysics,* **135,** 47–66.

Seront, B., Mainprice, D. & Christensen, N. I., 1992. A determination of the 3-dimensional seismic properties of an anorthosite—Comparison between values calculated from petrofabric and direct laboratory measurements, *J. geophys. Res.*, **98,** 2209–2221.

Shervais, J., 1979. Thermal emplacement model for the alpine lherzolite massif at Balmuccia, Italy, *J. Petrol.*, **20,** 795–820.

Siegesmund, S. & Kruhl, J. H., 1991. The effect of plagioclase textures on velocity anisotropy and shear wave splitting at deeper crustal levels, *Tectonophysics*, **191**, 147–154.

Siegesmund, S., Takeshita, T. & Kern, H., 1989. Anisotropy of V_p and V_s in an amphibolite of the deeper crust and its relationship to the mineralogical, microstructural and textural characteristics of the rock, *Tectonophysics*, **157**, 25–38.

Sills, J. D., 1984. Granulite facies metamorphism in the Ivrea Zone, NW Italy, *Schweiz. Mineral. Petrogr. Mitt.*, **64**, 169–191.

Silver, P. G. & Chan, W., 1988. Implications for continental structure and evolution for seismic anisotropy, *Nature*, **335**, 34–39.

Silver, P. G. & Chan, W. W., 1991. Shear wave splitting and subcontinental mantle deformation, *J. geophys. Res.*, **96**, 16 429–16 454.

Vaughan, M. T. & Guggenheim, S., 1986. Elasticity of muscovite and its relationship to crystal structure, *J. geophys. Res.*, **91**, 4657–4664.

Voshage, H., Hofman, A. W., Mazzuchelli, M., Rivalenti, G., Sinigoi, I., Raczeck, I. & Demarchi, G., 1990. Isotopic evidence from the Ivrea Zone for a hybrid lower crust formed by magmatic underplatting, *Nature*, **347**, 731–736.

Weidner, D. J. & Vaughan, M. T., 1982. Elasticity of pyroxenes: effects of composition versus crystal structure, *J. geophys. Res.*, **87**, 9349–9353.

Zingg, A., 1980. Regional metamorphism in the Ivrea Zone (Southern Alps, N-Italy): Field and microscopic investigation, *Schweiz. Mineral. Petrogr. Mitt.*, **60**, 153–179.

Zingg, A., Handy, M. R., Hunziker, J. C. & Schmid, S. M., 1990. Tectonometamorphic history of the Ivrea zone and its relationship to the crustal evolution of the southern Alps, *Tectonophysics*, **182**, 169–192.

Zubov, V. G. & Firsova, M. M., 1962. Elastic properties of quartz near the α–β transition, *Soviet Phys. Cryst., English translations*, **7**, 374–376.